Universidad Autónoma del Estado de México

Facultad de Química

Estudio y caracterización de nanopartículas de óxido de hierro funcionalizadas con Ácido fólico/Rodamina a través de una reacción de entrecruzamiento tipo Carbodiimida.

Tesis que para obtener el grado de:

Maestra en Ciencias Químicas

Presenta:

Q.F.B. Alejandra Ancira Cortez

Dirigido por:

Dr. en C.Q. Enrique Morales Avila (UAEMéx)
Dr. en C.Q.B. Carlos González Romero (UAEMéx)
Dr. en C. Erick Cuevas Yáñez (UAEMéx)

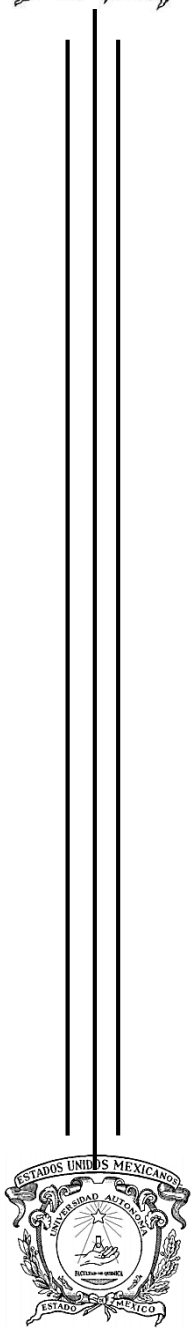

Toluca Estado de México, Julio de 2016

Contenido

Ancira-Cortez A.

RESUMEN

De acuerdo a estadísticas que indican que para el año 2012 la incidencia de cáncer a nivel mundial causó 8.2 millones de muertes, esta es considerada como una de las enfermedades con mayor incidencia en mortalidad, siendo los que más defunciones causan los cánceres de pulmón, hígado, estómago y colón. Es por ello que ciencias emergentes como la nanotecnología y las ciencias médicas, suman sus esfuerzos en el diseño de nuevas estrategias para diagnóstico temprano, tratamientos más eficaces y menos efectos indeseables.

Las nanopartículas de hierro han sido empleadas como medios de contraste y vectores ya que ofrecen útiles ventajas al poder ser sintetizadas a tamaños controlables y optimizables. En el presente trabajo se realizó la síntesis y caracterización de nanopartículas de óxido de hierro (IONPs) funcionalizadas con ácido fólico-rodamina a través de un método de co-precipitación y una reacción de carbodiimida.

Una vez sintetizado el sistema se realizó su caracterización mediante diferentes técnicas espectroscópicas y microscópicas para conocer sus características de forma, tamaño y composición; así como su caracterización biológica mediante ensayos de toxicidad y captación.

Al realizar lo anterior se pudo comprobar la correcta síntesis, así como las adecuadas características fisicoquímicas y biológicas del sistema para su uso como vector hacia receptores de folato a través del ácido fólico.

ABSTRACT

Cancer is one of the diseases with most deaths worldwide (around 8.2 million annually). For this reason, several treatments and diagnostic tools have been investigated and developed over the past decades.

Among them, the optical imaging systems result in a new area of investigation. In the present research a dual-image system has been developed to achieve and enhance the detection of cancer, which has not been done with systems currently available.

With the development of nanoformulations containing the aforementioned characteristics, researchers have explored the feasibility of improving the current drawbacks of cancer diagnosis, employing non-invasive systems for monitoring the disease in real time.

The present study describes the preparation of a dual-image targeting system composed of magnetic iron oxide nanoparticles which have been functionalized with folic acid and rhodamine isothiocyanate, were the nanoparticles synthesis was achieved by a co-precipitation method and the modification with the targeting molecule was carried out by a carbodiimide reaction.

Nanoparticles were characterized by spectrometric techniques and the toxicity and cellular uptake were evaluated. The multifunctional system showed suitable physicochemical and biological properties for cell-targeting through folate receptors.

MARCO CONCEPTUAL

1. ANTECEDENTES

Para el año 2008, se esperaba que el cáncer fuera casusa de más de 10 millones de diagnósticos en personas alrededor del mundo, además de más de 8.2 millones de muertes. El notable incremento en las cifras de personas con cáncer puede ser relacionado al hecho de que es fuertemente dependiente del desarrollo de nuevas tecnologías para su diagnóstico y tratamiento (Luo, Zhang et al. 2011, Mahmoudi, Sahraian et al. 2011, M., Park et al. 2012, Jang, Kwon et al. 2016). Razón por la cual la investigación científica se encuentra centrada en un porcentaje importante en atender este tipo de problemáticas

Aun cuando existen numerosos fármacos contra el cáncer, existen diversos problemas propios de estos; entre los principales están aquellos asociados a su administración sistémica; incluyendo la distribución general del mismo, la falta de especificidad hacia los sitios patológicos, la necesidad de concentraciones altas para lograr la adecuada concentración local, la toxicidad no específica, entre otros. (Mahmoudi, Sahraian et al. 2011, Jang, Kwon et al. 2016, Kanamala, Wilson et al. 2016). Aunado a esto, la falta de técnicas de diagnóstico temprano o adecuado, aumentan los valores de los indicadores epidemiológicos para esta enfermedad, tanto a nivel mundial como nacional.

Sin embargo, el desarrollo de nuevos sistemas o herramientas para un mejor y más adecuado tratamiento y diagnóstico de dicha enfermedad es hoy en día una amplia área de estudio e interés, para de esta manera poder hacer frente a dicha enfermedad. Este tipo de sistemas son conocidos o denominados como como *teranósticos* y ofrecen la posibilidad de integrar en un solo sistema tanto las ventajas de moléculas/fármacos para el tratamiento de la patología, así como las características de las herramientas de diagnóstico por imagenología (Janib, Moses et al. 2010, Kelkar and Reineke 2011, Choi, Liu et al. 2012, Fan, Fu et al. 2014).

En imagenología óptica existen diferentes modalidades que resultan ser prometedoras al ser no-invasivas, poder realizar el diagnóstico en tiempo real, además de ofrecer una alta resolución para la detección del cáncer (Ej. Imagenología por florescencia, RMI) (Luo, Zhang et al. 2011, Jang, Kwon et al. 2016).

1.1. Nanotecnología

La ciencia a nanoescala y la ingeniería nos proveen un entendimiento sin precedentes y un control de la materia a su nivel más fundamental: las escalas atómicas y moleculares (Mahmoudi, Sant et al. 2011). Hoy en día, este tipo de investigación y desarrollo tecnológico esta en arduo e intenso crecimiento.

Esta área es conocida como nanotecnología, y conduce a la creación de materiales y dispositivos útiles, y a la síntesis empleada para manipular y estudiar de manera controlada la materia a escalas que incluyen rangos de 1 a 100 nanómetros (Sinha, Kim et al. 2006, Cao, He et al. 2009, Gao and Xu 2009).

1.1.1. Nanotecnología aplicada a la medicina

La integración de la nanotecnología con la medicina ha resultado en el desarrollo activo de una nueva área de investigación; la nanomedicina. En la cual, diversas nanoestructuras (nanopartículas, nanocables, nanofibras, nanotubos, etc.) han sido estudiadas para distintas aplicaciones biológicas, por ejemplo: uso como biosensores, para separación biológica y en terapia contra el cáncer debido a la particularidad de sus nuevas propiedades y funciones que difieren drásticamente de las presentes en el material a macroescala (Adlim 2006, Gao and Xu 2009, Wooley 2011|).

Avances recientes en nanomateriales han explorado estrategias para la entrega pasiva y activa de los medicamentos, mejorando las concentraciones intratumorales de los fármacos al mismo tiempo que limitan la toxicidad en el tejido sano, así como en la obtención y creación de sistemas para el diagnóstico, entre los cuales se encuentran los sistemas para imagenología dual, mediante la obtención de imágenes a través de técnicas como la RMI y fluorescencia (M., Park et al. 2012, Yan, Wu et al. 2013, Wen, Jiang et al. 2014).

Diferentes tipos de materiales han sido estudiados y empleados para obtener nuevas estructuras útiles en la medicina, dentro de estos se encuentran las nanopartículas de óxido de hierro, que deben su interés a sus propiedades magnéticas y ópticas intrínsecas y a sus

interacciones con los sistemas biológicos; y que además ofrecen diversas oportunidades de estudio, los cuales se enfocan en examinar sus funciones en aspectos como el marcaje celular, la separación celular, la magnetofección, la entrega de fármacos, la inducción de hipertermia, la formación de imágenes de resonancia magnética como diagnóstico médico, como biosensores, etc. (Song, Wang et al. 2015, Das, Mishra et al. 2008, Gao and Xu 2009, Calmon, de Souza et al. 2012) .

1.2 Nanopartículas de óxido de hierro

Existen diferentes tipos de materiales (tanto de naturaleza orgánica como inorgánica) que han sido estudiados y empleados para obtener nuevas estructuras útiles y con aplicaciones biomédicas.

Los materiales empleados con estos fines normalmente están formados por núcleos magnéticos de elementos como Mn, Fe, Co, Ni, Gd, Mg y sus correspondientes óxidos (Zeinali Sehrig, Majidi et al. 2015, Calero, Gutierrez et al. 2014, Kelkar and Reineke 2011, Kumar and Mohammad 2011). En el grupo de materiales anteriormente mencionados se encuentran las nanopartículas de óxido de hierro (IONPs), en especial en su forma de magemita (Fe_3O_4); que deben su interés además de sus propiedades fisicoquímicas a su alta y comprobable biocompatibilidad en sistemas biológicos, conjuntamente, gracias a su magnetismo ofrecen diversas aplicaciones en biomedicina, ej. marcaje celular, separación celular, magnetofección, entrega de fármacos, inducción de hipertermia, formación de imágenes mediante Resonancia Magnética de Imagen (RMI), etc. (Das, Mishra et al. 2008, Gao and Xu 2009, Calmon, de Souza et al. 2012 Song, Wang et al. 2015).

1.2.1. Síntesis de las nanopartículas de óxido de hierro

Uno de los métodos de síntesis más ampliamente usados para la formación de IONPs es el método de co-precipitación .

La reacción general para la formación de nanopartículas de Fe_3O_4 es como se describe en la Ec. 1:

$$Fe^{2+} + 2Fe^{3+} + 8OH^- \rightarrow Fe_3O_4 + 4H_2O \qquad \text{Ec. (1)}$$

La generación de las nanopartículas bajo las condiciones ideales de síntesis se lleva a cabo por la formación de un núcleo cristalino delgado en un medio sobresaturado, seguido por el crecimiento cristalino. El último proceso es controlado por el transporte de masas y por el equilibrio de adición de superficie y la eliminación de los monómeros individuales; es decir, átomos, iones o moléculas. Por lo tanto, la fuerza impulsora de eliminación del monómero (disolución) aumenta con la disminución del tamaño de partícula. Así, dentro de un conjunto de partículas con tamaños ligeramente diferentes, el crecimiento de las partículas más grandes será a costa de las pequeñas, Este mecanismo se denomina maduración de Otswald y por lo general se cree que es la principal ruta de crecimiento de los cristales (Gupta and Gupta 2005).

1.2.2. Aplicaciones médicas de las nanopartículas de hierro

Las nanopartículas con propiedades magnéticas generan un amplio interés debido a sus aplicaciones en campos de tratamiento y diagnóstico de cáncer. Un ejemplo muy claro de estas son las nanopartículas magnéticas de óxido de hierro. Entre estás existen varios tipos de acuerdo a su conformación espacial. La maghemita γ-Fe_2O_3, magnetita β-Fe_3O_4, y hematita α-Fe_2O_3, de las cuales, la que destaca es la magnetita al ser muy competente debido a su probada biocompatibilidad (Rahman, Khan et al. 2012).

Algunas de las ventajas que ofrecen los materiales magnéticos en las aplicaciones biomédicas son: 1) ofrecen tamaños controlables que van desde unos pocos hasta decenas de nanómetros, por lo que su optimización de tamaño y propiedades fácilmente coinciden con el interés del estudio; 2) las nanopartículas pueden ser manipuladas por fuerzas magnéticas externas y 3) juegan un papel importante como agentes de contraste en MRI debido a que la señal del momento magnético de un protón alrededor de las nanopartículas magnéticas puede ser capturado por resonancia de absorción.

La clave del éxito de las aplicaciones de las nanopartículas magnéticas es su modificación superficial debido a que necesitan una superficie compatible para interactuar con las células o en otros casos mejorar sus características y cualidades para obtener las funciones deseadas del sistema. Este tipo de modificaciones se pueden realizar con diferentes compuestos, entre los que se encuentran como ejemplo, anticuerpos, péptidos, moléculas pequeñas, o aptámeros (Das, Mishra et al. 2008, Gao and Xu 2009, Calmon, de Souza et al. 2012).

Algunas de las razones para funcionalizar las nanopartículas son: 1) prevenir su agregación durante los largos periodos de almacenamiento, 2) mantener una adecuada solubilidad, 3) mantener las propiedades de los nanomateriales y 4) asegurar su biocompatibilidad después de que interactúan con su sitio blanco (Das, Mishra et al. 2008, Gao and Xu 2009, Das, Bandyopadhyay et al. 2011).

Por su propiedad de responder a campos magnéticos, las nanopartículas magnéticas funcionalizadas tienen dos características: especificidad y magnetismo, lo cual nos lleva a diversas aplicaciones como la unión y orientación específica para detección de bacterias, purificación de proteínas, descontaminación de tóxicos y uso en colorantes o fármacos (Gao and Xu 2009).

Un aspecto importante en las nanopartículas de hierro funcionalizadas es su capacidad de multivalencia, es decir varios ligandos con propiedades terapéuticas, de diagnóstico, o propiedades de barrera, pueden ser incorporados sobre la superficie de la nanopartícula; todo en un solo sistema. Esta focalización multivalente aumenta significativamente la afinidad de unión de una partícula hacia una célula blanco a una escala molecular (Fasting, Schalley et al. 2012).

1.2.3. Sistemas basados en nanopartículas de óxido de hierro para aplicaciones biomédicas.

Algunos de los estudios previos que emplean como núcleo a nanopartículas de hierro para aplicaciones médicas se encuentran descritos en la Tabla 1.

Tabla 1. Sistemas basados en nanopartículas de hierro para aplicaciones biomédicas

Núcleo	Descripción del sistema	Uso	Autores
Fe_3O_4 20 nm	FA-MNP's AF adsorbido a las Fe_3O_4.	Evaluar el efecto de FA-MNP's en combinación con ELF-EMF para apoptosis de células de cáncer de hígado BEL-7402. (EF: campos electromagnéticos, ELF: Frecuencias extremadamente bajas).	(Wen, Jiang *et al.* 2014)
Fe_3O_4 10 nm	IONP's-Tumastatin-Rodamina B Tumastatin acoplado vía carbodiimida.	Evaluar el efecto de la penetración selectiva en la vasculatura de la masa tumoral de glioma en un modelo tridimensional.	(Ho, Kohler *et al.* 2012)
Fe_3O_4 6 nm	ISA23SH:SPIO@PAA Copolímeros ISA23SH y PAA con fragmentos de $Re(CO)_3$ adsorbidos a Fe_3O_4.	Evaluar su probable uso como agentes de contraste de RMI debido a sus propiedades magnéticas.	(Maggioni, Arosio *et al.* 2014)
Fe_3O_4 13 nm	β-Ciclodextrina-IONP-amino-silano (3-aminopropil)triethoxisilano con β-ciclodextrina para cubrir Fe_3O_4 mediante el método de capa por capa	Evaluar las características del sistema para futuras aplicaciones como acarreador de fármacos mediante manipulación de campos magnéticos.	(Cao, He *et al.* 2009)
Fe_3O_4 90 nm	IONP-FA-RITC-PTX AF, PTX y RITC conjugados a nanopartículas de Fe_3O_4 mediante química click.	Uso de ácido fólico como vector en células cancerosas que sobreexpresan receptores de folato, induciendo apoptosis mediante selectividad específica a diferencia del fármaco libre, evaluado mediante fluorescencia y RMI.	(Das, Bandyopadhya y *et al.* 2011)
Fe_3O_4 89 nm	IONP's Obtención de nanopartículas de Fe_3O_4 por coprecipitación.	Evaluar la eficiencia de transfección y citotoxicidad en células HeLa.	(Calmon, de Souza *et al.* 2012)
Fe_3O_4 30nm	DIONP's Dextrán adsorbido a Fe_3O_4.	Evaluar la citotoxicidad y ensayos de adhesión en cultivos de células de fibroblastos.	(Easo *et al.*, 2012).
Fe_3O^4 13 nm	IONPs-PEO- Rhd PEO (poli (etilen oxido)) acoplado a Fe_3O_4 y posterior enlace de Rdh mediante reacciones click ortogonales.	Evaluar el efecto de hipertermia de nanopartículas magnéticas y su seguimiento mediante fluorescencia.	(Guyen *et. al.*, 2013).
Fe_2O_3 10 nm	γ-Fe_2O_3-PEI, γ-Fe_2O_3-PEGPEI Núcleos de Fe_2O_3 con coraza de PEI y PEGPEI mediante adhesión.	Evaluar el efecto de RMI y la citotoxicidad en la línea celular A549 de adenocarcinoma de pulmón humano.	(Schweiger, Pietzonka *et al.,* 2011)
Fe_3O_4 11 nm	^{99m}Tc-SPION's SPION's cubiertas con PEG y radiomarcadas con ^{99m}Tc por adhesión.	Evaluar INOP's radiomarcadas como agentes en SPECT/MRI para observar su acumulación en nodos linfáticos.	(Madru, Kjellman *et al.* 2012)
Fe_3O_4 20 nm	Fe_3O_4PLGA:PEG_{4000}-DOX Estructura núcleo-coraza mediante una doble emulsión (w/o/w).	Evaluar la liberación del sistema creado así como realizar ensayos de citotoxicidad en la línea celular A549 de cáncer de pulmón.	(Akbarzadeh, Mikaeili *et al.* 2012)
Fe_3O_4 50 nm	TAT-SPION's	Evaluar el efecto del péptido TAT en la internalización de complejo multifuncional usando tomografía electrónica 3D en células de glioma.	(Nair, Fukuda *et al.* 2012)

Ancira-Cortez A.

1.3. Vectorización/ Funcionalización

Con la vectorización se pretende realizar la entrega y/o liberación de la(s) nanopartícula(s) multifuncional(es) a un sitio de acción, con el empleo de concentraciones más bajas a las normalmente usadas en un tamaño mayor, con la finalidad de magnificar los efectos terapéuticos y reducir los efectos adversos (Bennett, Jo et al. 2014).

1.4. Ácido fólico y cáncer

1.4.1. Descripción del ácido fólico

El ácido fólico (AF) es una vitamina de origen natural soluble en agua. Su deficiencia conduce a problemas de salud como anemia, depresión y defectos del cerebro. Algunos grupos funcionales que contiene son amino, imino, carboxilo, hidroxilo, imida y una amina terciara (Palanikumar, Kannammal et al. 2014). En su estructura básica está formado por un anillo de pteridina, un ácido p-aminobenzóico y un ácido glutámico (Castillo, Rindzevicius et al. 2015), como se puede observar en la Figura 1.

Los folatos (Vitamina B9) son importantes donadores de un carbono en la síntesis de purinas y timidinas; componentes esenciales en la síntesis de los ácidos nucleicos; en la replicación, la división celular, el crecimiento y la supervivencia, en particular de las células que se dividen rápidamente; e indirectamente participa en la vía S-adenosil para la metilación de ADN, ARN, proteínas y lípidos (Lu and Low 2002, Kelemen 2006, Chen, Ke et al. 2013, Castillo, Rindzevicius et al. 2015).

Diferentes estudios han demostrado que los folatos juegan un papel clave para la supervivencia y proliferación celular, mientras que el deterioro de los sistemas dependientes de folato provoca una serie de condiciones fisiopatológicas. Debido a la naturaleza hidrofílica de los folatos son necesarios mecanismos de transporte activos para permitir la absorción de estos por las células (Muller and Schibli 2011).

Aunado a lo anterior, los folatos resultan atractivos para ser empleados como moléculas de vectorización debido a que presentan una alta afinidad de unión a su receptor (K_d~10^{-10}M), , baja inmunogenicidad, facilidad de modificación, un tamaño pequeño (M_r 441.4), estabilidad durante su almacenamiento, compatibilidad con una gran variedad de solventes orgánicos y acuosos, un bajo costo y alta disponibilidad (Lu and Low 2002, Castillo, Rindzevicius et al. 2015).

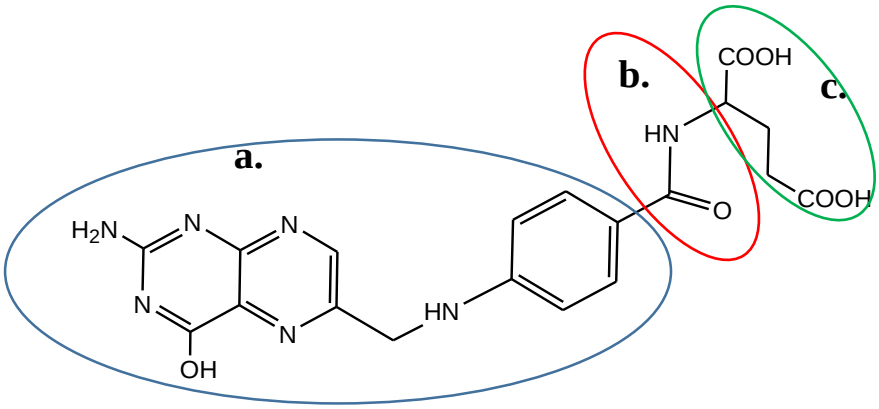

Figura 1. Estructura del ácido fólico, en el cual se muestran los sitios a. Sitio de reconocimiento biológico, b. Sitios que maximizan la afinidad y c. Sitio idóneo para la funcionalización.

1.4.2. Receptores de Ácido Fólico

Los receptores de folato (FR_α, FR_β y FR_γ) son glicoproteínas de superficie ricas en cisteínas, que unen con gran afinidad al folato mediando su captación celular (Chen, Ke et al. 2013).

En las células normales, el transporte se lleva a cabo principalmente a través del trasportador reducido del folato y el transportador de folato acoplados a protones. El tercer sistema de captación es la alta afinidad de sus receptores (FR), en el que una glicoproteína de glicosil fosfatidil inositol y una de 5-metiltetrahidrofolato se unen preferentemente al ácido fólico, el cual es internalizado posteriormente vía endocitosis (Muller and Schibli 2011).

Aunque se expresan a muy bajas concentraciones en la mayoría de los tejidos, los receptores de folato, especialmente FRα, se sobreexpresan en numerosos tipos de cánceres para satisfacer la demanda de folato de las células con altas tasas de proliferación (Lu and Low 2002, Chen, Ke et al. 2013). En la figura 2 se muestra la estructura tridimensional del receptor de folato, así como la distribución de las cargas de su superficie.

Por otro lado, constituyen un blanco útil para la administración de fármacos específicos en los tumores, principalmente porque: 1) estos están regulados positivamente en muchos cánceres humanos, incluyendo tumores malignos de ovario, cerebro, riñón, mama, células mieloides y de pulmón, 2) el acceso a los receptores de folato en los tejidos normales que los expresan puede ser severamente limitado, debido a su ubicación en la membrana epitelial apical polarizada (externamente orientada) y 3) la densidad de receptor de folato parece aumentar a medida que la etapa/ grado del cáncer avanza (Lu and Low 2002, Kelemen 2006).

La dependencia de folato de muchos procesos tumorales ha sido terapéutica y diagnósticamente explotada mediante la administración de anti-anticuerpos FRα, antifolato con alta afinidad, imágenes basadas en agentes de folato y la conjugación de fármacos y toxinas con el folato (Chen, Ke et al. 2013).

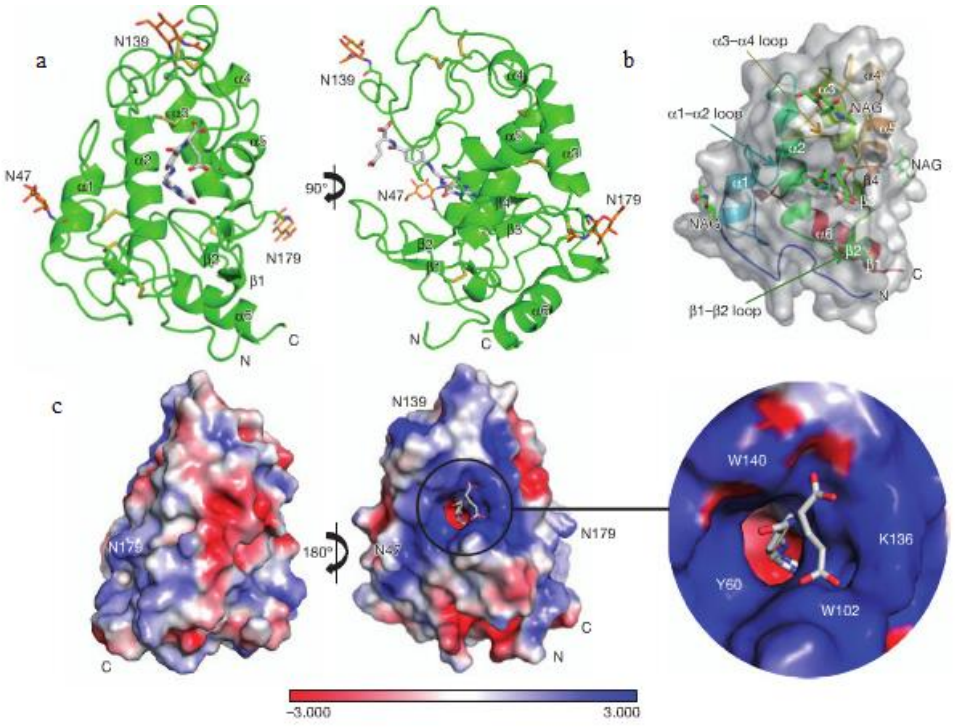

Figura 2. a. Vistas del complejo con el FRα en verde y el ácido fólico en gris. **b.** Diagrama de listón del FRα con el AF y NAG en verde superpuesto con la superficie del receptor. **c.** Distribución de las cargas de superficie del FRα con un acercamiento de la entrada al receptor, los átomos de carbono del ácido fólico están en gris, del nitrógeno en azul y del oxígeno en rojo. La barra de escala de color muestra una escala electrostática de -3 a +3 eV (Chen, Ke et al. 2013).

Ancira-Cortez A.

1.4.3. Sobreexpresión de receptores de ácido fólico en células tumorales

En tejidos sanos, la expresión de receptores de folato está restringida a los pulmones, los riñones, la placenta y el plexo coroideo. Los receptores de folato están presentes de manera importante en un gran número de cánceres epiteliales, incluyendo tumores de ovario, cérvix, endometrio, pulmón, pecho, colón y cerebro como se muestra en la Tabla 2 y la Tabla 3 (Muller and Schibli 2011).

Tabla 2. Expresión de receptores de folato (subtipos) en humanos en condiciones normales (Kelemen 2006)

	Tipo de tejido/sistema	Tipo de receptor		
		FRα	FRβ	FRγ
Tejido normal	Sistema genitounitario	• Placenta • Riñón • Vejiga	Placenta	
	Sistema nervioso central	• Plexo coroideo • Líquido cefalorraquídeo		
	Sistema Hematopoyético		• Baso • Timo • Neutrófilos	Células hematopoyéticas
	Sistema gastrointestinal.	Glándulas salivales submandibulares		
	Sistema respiratorio	Pulmón		

Tabla 3. Expresión de receptores de folato (subtipos) en procesos oncológicos con alta y baja expresión (Kelemen 2006)

	Tipo de expresión	Tipo de receptor		
		FRα	FRβ	FRγ
Tejidos malignos.	Alta expresión	• Leucemia • Carcinoma no mucinoso de ovario • Linfoma • Carcinoma cervical • Carcinoma uterino • Carcinoma primario de células renales	Leucemia	Leucemia
	Baja o imperceptible expresión.	• Carcinoma endotelial primario • Carcinoma primario de vejiga • Carcinoma primario de páncreas • Carcinoma colonorectal • Carcinoma primario de próstata • Carcinoma primario en cuello		

Ancira-Cortez A.

1.5. Colorantes de Rodamina

Los colorantes de Rodamina son fluoróforos pertenecientes a la familia de los xantenos, junto con los colorantes de fluoresceína y eosina (Beija, Afonso et al. 2009). La estructura general de los cromóforos de xanteno y de los colorantes de rodamina se muestran en la figura 3 y figura 4 respectivamente.

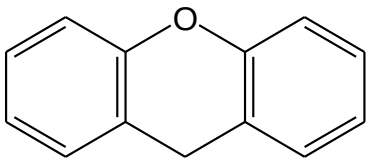

Figura 3. Estructura molecular de los cromóforos de xanteno

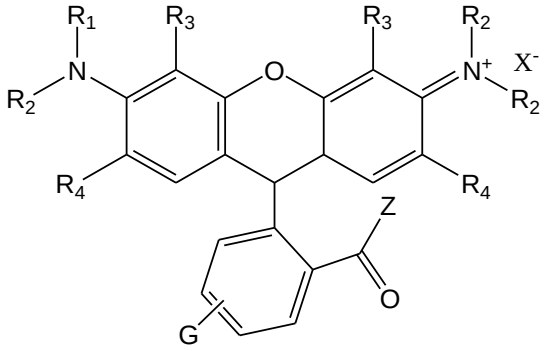

Figura 4*:* Estructura molecular de los colorantes de rodamina, donde G: un grupo funcional del tipo éster activado, cloruro de acilo, cloruro de sulfonilo o isotiocianato y X-: usualmente Cl^-, Br^- o ClO_4^-.

Dependiendo de los sustituyentes en R_1, R_2, R_3 y R_4, G, e incluso el contraión X-, los colorantes de rodamina presentan diferentes propiedades fotofísicas en solución, como las de absorción y emisión máxima (λ_{abs}^{max}, λ_{em}^{max}), tiempo de vida media de fluorescencia (τ) y rendimiento cuántico de fluorescencia (Φ) (Beija, Afonso et al. 2009).

Por su excelente fotoestabilidad y sus propiedades fotofísicas, las rodaminas son usadas como colorantes láser, estándares de fluorescencia (para rendimiento cuántico y polarización), como sondas de fluorescencia, así como para la detección de polímeros bioconjugados, imágenes de una sola molécula y en la formación de imágenes en las células vivas como un método de diagnóstico en diferentes enfermedades, basado principalmente en nanomateriales debido a su sencillez y sensibilidad (Song, Wang et al. 2015, Beija, Afonso et al. 2009).

1.5.1. Isotiocianato de Rodamina como molécula de marcado para imagen óptica

Recientemente, se han usado nanomateriales fluorescentes en bioanálisis y bioimagen, ya que muestran muchas ventajas sobre los enlaces convencionales de fluorocromo (Xie et al., 2013).

Los colorantes de rodamina, pertenecientes a la familia de los xantenos, son ampliamente utilizados como sondas fluorescentes debido a su alto coeficiente de absorción y emisión de fluorescencia en la región visible del espectro electromagnético, a su alto rendimiento cuántico de fluorescencia y a su fotoestabilidad (Beija, Afonso et al. 2009). El Isotiocianato de Rodamina B (IRDB) es una molécula adecuada para imagen óptica por sus propiedades fotofísicas satisfactorias (figura 5). Así mismo, se distribuye ampliamente a través de la membrana biológica en respuesta al potencial transmembranal, acción característica en cationes lipofílicos (Reungpatthanaphong, Dechsupa et al. 2003, Xie, Chang et al. 2013).

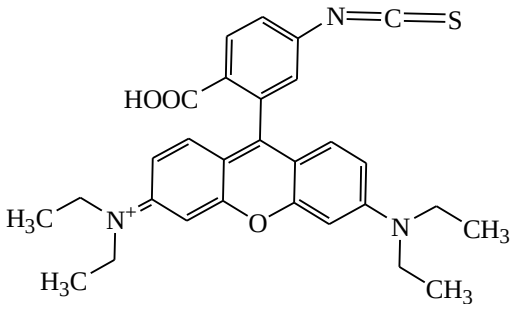

Figura 5. Estructura de la molécula de isotiocianato de Rodamina B.

JUSTIFICACIÓN

2. JUSTIFICACIÓN

Debido a la importancia que genera el cáncer en el sector salud como una significativa causa de muerte y a los tratamientos hasta hoy en día poco específicos para discernir entre células cancerosas y sanas, en el presente trabajo de investigación se llevó a cabo la síntesis de nanopartículas de óxido de hierro que fueron funcionalizadas mediante la reacción de adición y entrecruzamiento tipo carbodiimida, con ácido fólico y rodamina para su posible aplicación en biomedicina.

HIPÓTESIS

3. HIPÓTESIS

El sistema de nanopartículas de óxido de hierro modificado con rodamina y funcionalizado con ácido fólico (AF-Fe_3O_4-IRDB) podrá ser sintetizado de manera adecuada empleando una reacción de adición tipo carbodiimida, puesto que este tipo de reacciones han demostrado ser adecuadas y óptimas para la síntesis de conjugados con aplicaciones médicas, por lo cual será útil en la obtención del sistema multifuncional propuesto, resultando en la síntesis de precursores de vectorización aplicables en las ciencias médicas.

OBJETIVOS

4. OBJETIVOS

4.1. Objetivo general

- Sintetizar y caracterizar el sistema multifuncional de nanopartículas de óxido de hierro funcionalizadas con ácido fólico y rodamina B a través de una reacción de entrecruzamiento tipo carbodiimida.

4.2. Objetivos específicos

- Sintetizar y caracterizar nanopartículas de óxido de hierro (IONPs), por una reacción de coprecipitación de sales de hierro.
  - Modificar la superficie de las nanopartículas de óxido de hierro con ácido 2-amino-etilfosfónico (2-AEF).
  - Sintetizar y caracterizar el conjugado IONPs-ácido fólico (AF) por la reacción de entrecruzamiento y adición con carbodiimida.
  - Sintetizar y caracterizar el conjugado IONPs-rodamina B (IRDB) por la reacción de entrecruzamiento y adición con carbodiimida.
  - Sintetizar y caracterizar el conjugado IONPs-AF-IRDB por la reacción de entrecruzamiento y adición con carbodiimida.
- Evaluar la toxicidad inducida por el sistema multifuncional AF-IONPS-IRDB en cultivos celulares.
- Evaluar la captación celular del sistema *in vitro.*

METODOLOGÍA

5. METODOLOGÍA

5.1. Síntesis de las nanopartículas de óxido de hierro (IONPs).

La metodología que se realizó fue:

Se pesó y disolvieron 0.5g (0.005 mol) de $FeCl_2 \cdot 4H_2O$ en 10 mL de HCl 1M, se agregaron 1.35g (0.01 mol) de $FeCl_3 \cdot 6H_2O$ y se agitó la solución durante 30 min. Se añadió solución de NaOH 2M por goteo hasta un pH aproximado de 13, inmediatamente después se formó un precipitado negro. Se separó el precipitado mediante decantación magnética y se lavó con agua desionizada y desoxigenada hasta pH neutro. Finalmente, las nanopartículas de Fe_3O_4 (IONPs) se resuspendieron en agua destilada y desionizada.

5.2. Modificación superficial de las IONPs con ácido 2-aminoetilfosfónico (IONPs-2-AEF).

Para realizar la modificación de las nanopartículas con ácido 2-amino-etilfosfónico se realizó lo siguiente: Se hizo reaccionar 1 mmol de magnetita (Fe_3O_4) con 0.25 mmol de ácido 2-amino-eilfosfónico (2-AEF) y se colocó en ultrasonido la suspensión durante 1 h. Se separaron y recuperaron las nanopartículas modificadas mediante decantación magnética y se lavaron 3 veces con agua desionizada y desoxigenada. Se resuspendió el precipitado en agua desoxigenada y desionizada. Ver figura 6.

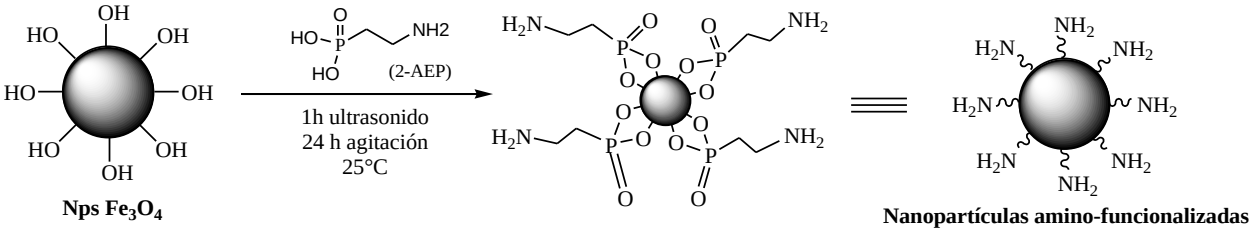

Figura 6. Reacción de funcionalización superficial de las nanopartículas de Fe_3O_4 con ácido 2-amino-etilfosfónico.

Ancira-Cortez A.

5.3. Conjugación con Rodamina B (IONPs-IRDB)

Para la síntesis del sistema IONPs con isotiocianato de rodamina B (IRDB) la metodología que se siguió fue la siguiente: Se preparó una solución acuosa de nanopartículas de óxido de hierro modificadas con 2-AEF (~25 mg) y se homogeneizaron usando ultrasonido durante 10 min. Se disolvió por otra parte IRDB (0.25 mM) en 10 mL de DMSO y se agregó la solución de IRDB por goteo a la suspensión acuosa. Posteriormente, se colocó en ultrasonido la suspensión resultante durante 1 h en oscuridad. Se recuperaron las nanopartículas de magnetita por decantación magnética y se lavaron exhaustivamente con agua desionizada (Fig. 7).

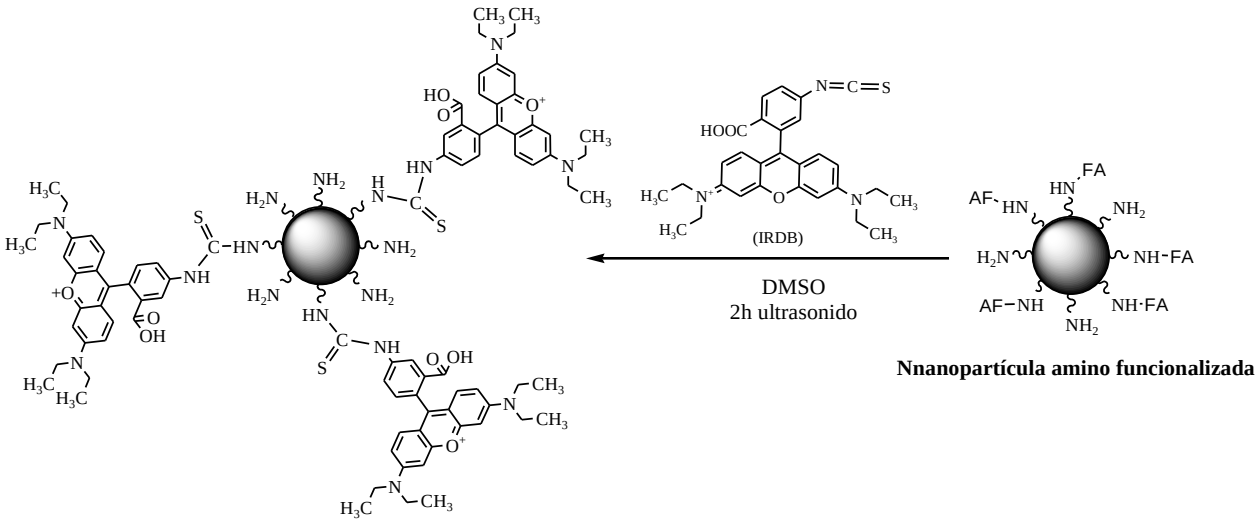

Figura 7. Reacción de conjugación de IONPs-2-AEF con isotiocianato de rodamina B.

5.4. Conjugación con Ácido Fólico (IONPs-AF)

Para la síntesis del sistema IONPs con ácido fólico (AF) la metodología a seguir fue la siguiente: Se disolvió el ácido fólico (2.5 mM) en aproximadamente 5 mL de DCM (diclorometano), se mezcló la solución anterior con una de EDC (1-etil-3-(3-dimetilaminopropil)carbodiimida) (75 mM) y DMAP (4-dimetilaminopiridina) (15 mM). Se añadió a la solución anterior alrededor de 200 mg de nanopartículas funcionalizadas con ácido 2-aminoetilfosfónico y se agitó la mezcla durante toda la noche a 37°C en oscuridad. Concluida la agitación se recuperó el precipitado magnéticamente y se lavó 3 veces con EtOH y posteriormente se lavó 5 veces con agua desionizada, finalmente se redispersaron las nanopartículas en agua desionizada (Figura 8).

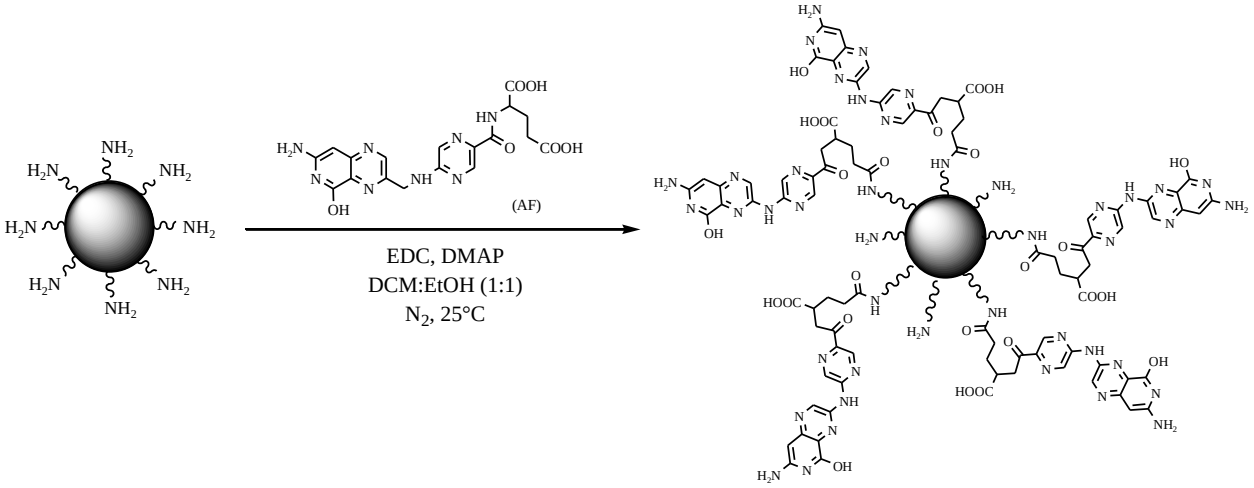

Figura 8. Reacción de conjugación de IONPs-2-AEF con ácido fólico.

5.5. Síntesis del sistema multifuncional (AF-IONPs-IRDB)

Para la síntesis del sistema IONPs con ácido fólico y rodamina B la metodología que se siguió fue la siguiente: Se disolvió IRDB a la concentración deseada en 10 mL de DMSO, se agregó esta solución por goteo a una suspensión acuosa de nanopartículas de óxido de hierro funcionalizadas con AF (IONPs-AF), posteriormente se colocó en ultrasonido la suspensión resultante durante 1 h, finalmente, se lavó exhaustivamente el sistema multifuncional de nanopartículas obtenido (AF-Fe_3O_4-IRDB) con agua desionizada *via* decantación magnética y se almacenó para análisis y estudios posteriores (Figura 9).

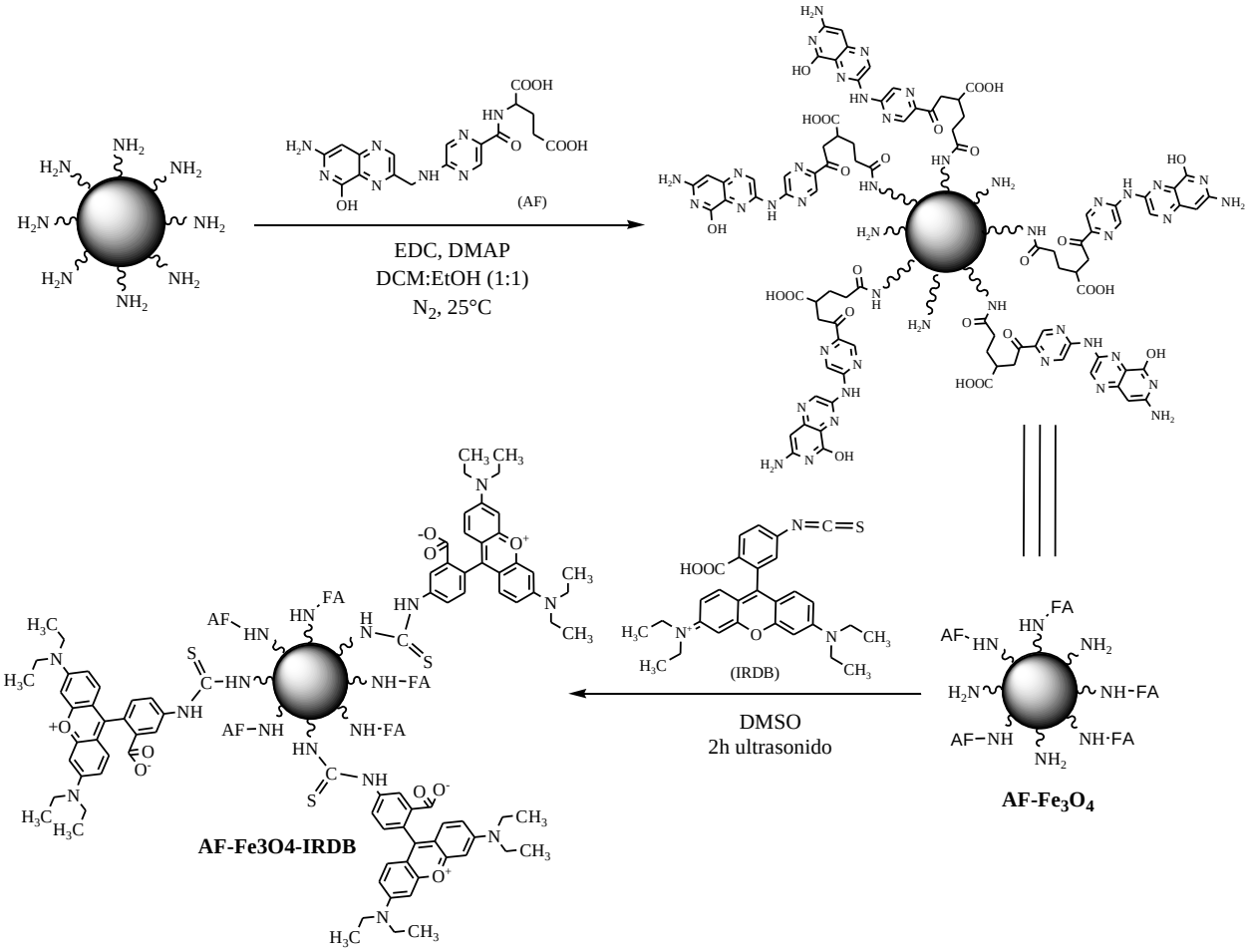

Figura 9. Reacción de conjugación de del sistema multifuncional de AF-IONPs-IRDB.

5.6. Caracterización

Se realizó la caracterización de los sistemas sintetizados mediante diferentes técnicas analíticas de acuerdo a lo descrito en la Tabla 4.

Tabla 4. Técnicas empleadas para la caracterización de los diferentes sistemas sintetizados

Sistema	DLS	FT-IR	Fluorescencia	UV-Vis	TEM	Raman
IONPs	✓	✓	✓	✓	✓	✓
IONPs-AEF	✓	✓				
IONPs- IRDB		✓	✓	✓		✓
IONPs-AF		✓	✓	✓		✓
AF-IONPs-IRDB		✓	✓	✓	✓	✓

5.7. Evaluación biológica

5.7.1. Estudios de citotoxicidad

Para evaluar la toxicidad del sistema multifuncional de nanopartículas de óxido de hierro con ácido fólico y rodamina se emplearon células HeLa, las cuales fueron cultivadas en placas de 96 pozos ($1x10^4$ células/pozo) usando 200 µL de medio RPMI libre de folatos suplementado con 10% de SFB y 100 unidades mL^{-1} de penicilina, 100 µg mL^{-1} estreptomicina y 0.25 µg mL^{-1} anfotericina B a 37°C en una incubadora con atmósfera de 5%-CO_2 95%-aire durante 24 h. Después de esto las células fueron tratadas con 20 µL a diferentes concentraciones del sistema multifuncional de nanopartículas de AF-Fe_3O_4-IRDB (0.5 mg mL^{-1}, 0.25 mg mL^{-1}, 0.125 mg mL^{-1} y 0.0625 mg mL^{-1}) y 180 µL de medio de cultivo, se incubaron durante 24 h a 37°C en una incubadora mantenida en condiciones atmosféricas de 5% CO_2-95%. Finalmente, se lavaron las células exhaustivamente con buffer de fosfatos pH 7.0 para eliminar completamente las nanopartículas no internalizadas. La viabilidad celular se evaluó empleando la tinción de cristal violeta, donde las células no tratadas con el sistema multifuncional de nanopartículas de AF-Fe_3O_4-IRDB se utilizaron como control (100% de viabilidad celular).

5.7.2. Estudios de captación

La captación celular se evaluó en células HeLa cultivadas en placas de 24 pozos, en las cuales se colocaron $5x10^5$ células/pozo a un volumen total de 2000 µL de medio libre de folatos suplementado con 10% SFB y 100 unidades mL^{-1} penicilina, 10 µg mL^{-1} estreptomicina y 0.25 µg mL^{-1} anfotericina B a 37°C y se mantuvieron en una incubadora con atmósfera de 5%-CO_2 95%-aire durante 24 h. Para poder determinar el porcentaje de captación por *via* receptores de ácido fólico se realizó un pre-tratamiento a un grupo de células, a las cuales se les colocaron 2 mL de una solución de AF a una concentración de 5 mg mL^{-1} y se mantuvieron durante dos horas en las células a las condiciones de incubación anteriormente descritas (para realizar el bloqueo de los receptores de AF), el otro grupo de células se incubó de igual manera, pero solamente con medio de cultivo (células sin bloqueo de recetores). Posterior a esto se retiró la solución y se lavaron las células pre-tratadas con buffer de fosfatos pH 7 tres veces, después de esto, se añadieron 40 µL del sistema multifuncional de nanopartículas a una concentración de 0.25 mg mL^{-1} en todas las células cultivadas y se incubaron durante 24 h a 37°C bajo las mismas condiciones anteriormente descritas. Finalmente, se separaron los sobrenadantes y se leyeron mediante espectroscopía UV-Vis y se determinó el porcentaje de captación en los dos diferentes grupos (con bloqueo y sin bloqueo).

RESULTADOS

[CPD] Submission Acknowledgement | BSP-CPD-2016-944

Gente

Current Pharmaceutical Design <cpd@benthamscience.org> Hoy a las 18:59

Para Dr. Enrique Morales-Avila

Reference#: BSP-CPD-2016-944
Submission Title: Preparation and Characterization of a Tumor-Targeting Dual-Image System based on Iron Oxide Nanoparticles Functionalized with Folic Acid and Rhodamine

Dear Dr. Enrique Morales-Avila,

Thank you for your submission to Current Pharmaceutical Design. It will be sent to the Editor in Chief for his approval, and once this is obtained for peer-reviewing, on the understanding that the manuscript contains original work that has neither been published earlier nor has simultaneously been submitted elsewhere. In case this is not so, please let us know immediately.

Please note that Bentham Science uses **CrossCheck's iThenticate software** to check for similarities between the submitted and already published material to minimise any chances of plagiarism.

Further, as per Bentham Science's **Ethical Guidelines for Publication,** all mansuscript are processed with the understanding that all authors and co-authors have reviewed and accordingly approved the manuscript before final submission to avoid any conflicts of interest later. Our ethical policies can be viewed at: http://benthamscience.com/journal/publishing-ethics.php?journalID=cpd#top.

In case of any doubt or conflict please contact us immediately.

Your manuscript has been assigned to the following Editor/Manager, to whom all correspondence is to be addressed:

Name:William Banks
Affiliation: VAPSHCS/GRECC S-182
Email:cpd@benthamscience.org
Looking forward to the successful publication of your article.

In case of delay, please feel free to write info@benthamscience.org

Sincerely,
Editorial Office
Bentham Science Publishers
Current Pharmaceutical Design
http://bsp-cms.eurekaselect.com/index.php/CPD

Preparation and Characterization of a Tumor-Targeting Dual-Image System based on Iron Oxide Nanoparticles Functionalized with Folic Acid and Rhodamine

Alejandra Ancira-Cortez[a], Enrique Morales-Avila[a*], Blanca E. Ocampo-García[b], Carlos González-Romero[a], Luis A. Medina-Velázquez[c], Gustavo López-Téllez[a], Erick Cuevas-Yáñez[a]

[a]*Facultad de Química, Universidad Autónoma del Estado de México, Toluca, Estado de México 50120, MÉXICO;* [b]*Instituto Nacional de Investigaciones Nucleares, Departamento de materiales Radiactivos, Ocoyoacac, Estado de México 52750, MÉXICO;* [c]*Unidad de investigación Biomédica en Cáncer, Instituto Nacional de Cancerología, Tlalpan, Sección XVI, Ciudad de México, 14080, MÉXICO.*

Abstract: Cancer is one of the diseases with most deaths worldwide (around 8.2 million annually). For this reason, several treatments and diagnostic tools have been investigated and developed over the past decades. Among them, a dual-image system has been developed to achieve and enhance the detection of cancer, which has not been done with systems currently available. With the development of nanoformulations with the aforementioned characteristics, researchers have explored the feasibility of improving the current drawbacks of cancer diagnosis employing non-invasive systems for monitoring. The present study describes the preparation of a dual-image targeting system composed of magnetic iron oxide nanoparticles with folic acid/rhodamine, achieved by a co-precipitation method for cancer cells. The multifunctional system was developed and characterized, and results showed suitable physicochemical and biological properties for cell-targeting through folate receptors. Also, a significant selectivity and uptake, facilitated by surface modification of iron oxide nanoparticles with folic acid, was demonstrated.

Keywords: Iron oxide nanoparticles, dual-imaging targeting, folic acid, folate receptor targeting, multifunctional nanoparticles.

1. INTRODUCTION

Molecular imaging comprises the non-invasive monitoring of functional and spatiotemporal processes at cellular, sub-cellular or molecular levels in humans and other living systems. Although molecular imaging has existed for decades, recent advances in molecular and cell biology, imaging technology, and material sciences have greatly increased its power and potential as specific and sensitive medical tools [1].

Nanoparticles (NPs) are submicron moieties with diameters ranging from 1 to 100 nm, depending on their intended purpose [2, 3]. They are obtained from inorganic or organic materials [2-4] which have many novel physical and chemical properties that are not present in the atom nor the bulk counterpart, related to the dimensions and shape, as well as morphology [1-3,7.8]. NPs has been used in many different biological and medical applications as key components for imaging probe design [2, 6, 9-24].

Iron oxide magnetic nanoparticles (IONPs) of magnetite type (Fe_3O_4) have desirable physical and biochemical characteristics (e.g. superparamagnetism, high coercivity, low Curie temperature (T_C), high magnetic susceptibility chemical stability in physiological conditions, high saturation fields, biocompatibility, biodegradable and non-toxic nature) [2, 5, 13, 16, 23-30], which make them useful in the diagnosis and treatment in the oncology field.

A desirable molecular imaging probe must be able to reach specific targets with high affinity, sensitivity and suitable biodistribution properties. Nanoparticle-based molecular imaging probes can be functionalized or modified due to their high surface area-to-volume ratio, by bioactive molecules, typically through chemical coupling *via* amide or ester bonds in order to reach a target site [3, 5, 15, 23, 31-33]. Some of the molecules used as targeting elements include small ligands, antibodies and derivatives, aptamers and other nucleic acids, polyunsaturated fatty acids, peptides and proteins [3,5,13,31]. Furthermore, surface modification can include fluorescence dyes, genes or drugs, to provide multimodal functionalities [7].

Folic acid (FA) is a water-soluble vitamin, formed by a pteridine ring (pt), *p*-aminobenzoic acid (paba) and glutamic acid (GA) [34], lacks immunogenicity, has high stability, low cost, small size (M_r= 441.4), low molecular weight, compatibility with a variety of organic and aqueous solvents, can be easily conjugated to supramolecular and macromolecular structures and has been used as a vector for cancer cells targeting due to its high affinity ($K_d \sim 10^{-10}$ mM) for its corresponding folate receptors (FRs: FR_α, FR_β and FR_γ), to mediate cellular uptake of FA [2, 5, 13, 16, 23, 30-31, 34-35, 37-41].

*Address correspondence to this author at the Facultad de Química, Universidad Autónoma del Estado de México, C.P. 50120, Toluca, México; Tel: +52-722-2-17-41-20 (ext. 134); Fax: +52-722-2-17-38-90; E-mails: enrimorafm@yahoo.com.mx; emoralesav@uaemex.mx

FRs are overexpressed in a large number of cancer cells [7, 31, 35-38, 41-42], and are positively associated with tumor stage and histologic grade (e.g. ovarian cancer, endometrial cancer, kidney cancer, colorectal cancer, lung cancer, breast cancer, brain cancer, myeloid leukemia) [36, 37, 43]. FRs provide a special marker that distinguishes cancer cells from normal cells, as these exhibit limited expression, are largely restricted to those important for embryonic development (e.g. placenta and neural tubes), and present low levels in folate resorption through kidney and lung [31, 37-42, 44]. It has been reported that folate conjugation to the IONPs enhances the cellular uptake to target cells, improving therapeutic efficacy [31].

Rhodamine B isothiocyanate, on the other hand, is a fluorophore that belongs to the xanthene dyes family [45-47]. Due to their photophysical properties and excellent photostability, they are used as fluorescence probes for imaging in living cells among other applications, such as laser dyes, fluorescence standards, pigments and so on [45, 30].

The term *theranostic nanoparticles* (TNPs) refers to multifunctional nanomaterials that combine diagnosis and therapy [17, 32, 48, 49]. Optical imaging allows non-invasive drug visualization in cells and tissues in order to understand molecular processes in real time. Specifically, it has been reported that several MNPs (Magnetic Nanoparticles) can be used as dual-modality imaging probes, in nuclear and optical fluorescence imaging [15, 17, 30, 50-52].

The modalities currently available are: a) Fluorescence imaging (FI), widely used due to its deep tissue penetration, low background interference, low aggregation tendencies, low cytotoxicity, high quantum yield, inherent simplicity and sensitivity, and *in vivo* stability [15, 33, 50, 51, 53-54]; b) Magnetic Resonance Image (MRI), based on the precession of water hydrogen nuclei within an applied magnetic field [48, 55], is a technique which allows physiological and anatomical monitoring details with good spatial resolution and measurement of biological processes at the molecular and cellular levels [15, 56], where IONPs are used as contrast agent, especially for transverse relaxation time T_2/T_2^* appropriate for the early cancer diagnosis. Furthermore, modalities such as single-photon emission computed tomography (SPECT) and single positron emission tomography (PET) are widely used for the detection and staining of cancer [15].

Therefore, we aimed to develop a tumor-targeting dual-image system based on IONPs with folic acid as a vector and rhodamine isothiocyanate as an imaging agent, primarily designed for non-invasive monitoring, in order to acquire high-quality targeted images without cytotoxicity to normal cells.

2. MATERIALS AND METHOD

2.1. Materials:

All chemicals were of analytical grade from commercial sources used without further purification. Ferric chloride hexahydrate ($FeCl_3{\cdot}6H_2O$), ferrous chloride tetrahydrate ($FeCl_2{\cdot}4H_2O$), folic acid, *N*-(3-dimethylaminopropyl)-*N'*-ethylcarbodiimide hydrochloride (EDC), 4-(dimethylamino) pyridine (DMAP), 2-aminoethylphosphonic acid (2-AEP) and rhodamine B isothiocyanate mixed isomers (RITC) were purchased from Sigma-Aldrich® Chemical Co. (St. Louis, MO, USA). folate-free RPMI-1640 medium, bovine fetal serum, $NaHCO_3$, antibiotic-antimycotic solution (100X) containing penicillin, streptomycin and amphotericin, and other chemicals and solvents were of reagent grade. The HeLa cell line was obtained from the National Institute of Cancerology, Mexico.

2.2. Methods:

2.2.1. Size and morphology:

Nanoparticles were analyzed by TEM in a JEOL JEM 2010 HT microscope operating at 200 kV in order to observe the two-dimensional, relative size, and morphology of nanoparticles. Samples were prepared for analysis by evaporating a drop of aqueous product on a carbon-coated TEM copper grid.

2.2.2. Surface chemistry:

The successful synthesis of amine-nanoparticles, as well as their folate and rhodamine-linked counterparts were studied using a FT-IR spectrometer, UV-Vis spectrometer and a fluorescence spectrometer.

2.2.2.1. Infrared spectroscopy:

The IR spectra were acquired from vacuum-dried samples on a PerkinElmer System 2000 spectrometer with an ATR platform (Pike Technologies) by applying the Attenuated Total Reflection Fourier Transform Infrared (ATR-FTIR) spectroscopy with a 4 cm^{-1} resolution, 40 scanning, operating range 4000-40 cm^{-1}.

2.2.2.2. Raman Spectroscopy:

The Raman spectra of the dehydrated samples were acquired on a MicroRaman (JOBIN-Yvon-Horiba, LABRAM HR800) spectrometer with an optical microscopy (OLYMPUS BX 41), a He-Ne Laser (632.817 nm) as an excitation source, a D0.6 filter and a 200 μm hole. Fifteen/10 second scans were acquired. Samples were deposited on a cover glass and evaporated with vacuum at room temperature.

2.2.2.3. UV-Vis studies:

The absorption spectra, in the range of 200–700 nm, was obtained through a Thermo Genesys 10S spectrometer using a 1-cm quartz cuvette.

2.2.2.4. Fluorescence spectroscopy

The emission fluorescence spectra, in the range of 450-450 nm, was obtained through a Horiba Jovin Yvon Spectrofluorimeter (Fuoromax-P) with dual excitation and emission monochromators in a wavelength range between 350 and 800 nm. Nanoparticles were measured with a λ_{exc} of 398 nm using a 1-cm cuvette. Three/0.5 seconds scans were acquired.

2.2.3. Determination of the concentration of FA conjugated over the surface of the IONPs:

The number of FA molecules attached per nanoparticle was calculated by UV-Vis spectroscopy using different FA concentration, as in the carbodiimide reaction described in the experimental section. The employed FA concentrations were 2.5 mM, 5.0 mM, 6.3 mM, 7.5 mM, 8.8 mM and 10.0 mM.

Nanoparticles were measured after washing them with purified water. The concentration was calculated using the prepared standard curve (r^2= 0.9997, with excellent linearity from 0.0125 mM to 0.5 mM). The experiments were conducted in triplicate (n =3).

2.2.4. Concentration of RITC conjugated over the surface of the IONPs:

RITC conjugation were determined by titration using 0.0125 mM, 0.0375 mM, and 0.0625 mM RITC, employing the synthesis method described in the experimental section. Samples were washed with purified and deionized water, and the corresponding nanoparticles were measured by UV-Vis spectroscopy, calculating the concentration using the prepared rhodamine isothiocyanate standard curve ($r^2 \geq 0.9975$, with excellent linearity from 0.0033mM to 0.0673 mM). The experiments were conducted in triplicate (n =3).

2.2.5. Cell proliferation studies/ Nanoparticle-induced cytotoxicity:

HeLa (human cervix adenocarcinoma) cells ($1x10^4$ cells/well) were seeded onto a 96-well plate and cultured in 200 µL of folate-free RPMI medium containing 10% FBS, 100 units mL^{-1} penicillin, 100 µg mL^{-1} streptomycin and 0.25 µg mL^{-1} amphotericin B at 37°C in a humidified 5%-CO_2/95%-air atmosphere, and incubated for 24 h. The cells were treated with 20 µL of different FA-Fe_3O_4-RITC nanoparticle concentrations (0.5 mg mL^{-1}, 0.25 mg mL^{-1}, 0.125 mg mL^{-1} and 0.0625 mg mL^{-1}) and 180 µL of media culture were added, incubated for 24 h at 37°C in a humidified incubator maintained at 5% CO_2/95% air atmosphere. Thereafter, cells were washed thoroughly with PBS to remove the non-internalized nanoparticles. Cell viability was evaluated using a crystal violet staining. Untreated cells served as 100% viable cells.

2.2.6. Cellular Uptake:

Nanoparticle uptake by HeLa cells was evaluated using $5x10^5$ cells/well seeded onto 24-well plates and cultured in a total volume of 2000 µL of folate-free RPMI medium containing 10% FBS, 100 units mL^{-1} penicillin, 10 µg mL^{-1} streptomycin and 0.25 µg mL^{-1} amphotericin B at 37°C in a humidified 5%-CO_2/95%-air atmosphere and incubated for 24 h. After the period of incubation ended, 40 µL of nanoparticles, (at a concentration of 0.25 mg mL^{-1}) were added, incubated for 24 h at 37°C in a humidified incubator maintained at 5% CO_2/95% air atmosphere. The images for the cellular uptake test were obtained with an inverted confocal microscope, consisting of an Olympus IX80 with a Plan-Neofluar 40x, AxioVert (Carl Zeiss) objective and an Axio Vision software.

3. EXPERIMENTAL:

3.1. Synthesis of Magnetic Iron Oxide Nanoparticles (IONPs):

Bare magnetic iron oxide nanoparticles were synthesized by an alkaline co-precipitation of Fe^{3+} and Fe^{2+}, where 0.5 g (2.5 mM) of ferrous chloride tetrahydrate ($FeCl_2{\cdot}4H_2O$) was dissolved in 10 mL 1M HCl solution, and then 1.35 g (5 mM) of ferric chloride hexahydrate ($FeCl_3{\cdot}6H_2O$) was added to the solution before stirring for 30 min. Then ~15 mL of 2M NaOH solution was added until pH ~13. Immediately, a black precipitate appeared, indicating the formation of magnetite (Fe_3O_4). This black precipitate was separated via magnetic decantation and washed with deionized and deoxygenated water until neutral pH was reached. Finally, the IONPs were re-dispersed in deionized and deoxygenated water and stored for later use.

3.2. Surface modification with 2-aminoethylphosponic acid (2-AEP):

For surface activation, a freshly-prepared aqueous solution of 2-AEP (1 mM) was added to 4 mM of a colloidal suspension of magnetite nanoparticles with sonication using a high-intensity ultrasonic probe during an hour (see figure 1). Then, the resulting nanoparticle suspension was stirred vigorously with a magnetic stirrer at 25°C for 24 h. The particles were then washed with deionized water three times via magnetic decantation and finally dried by evaporation at 37°C. Samples were stored for posterior use (see figure 1a).

3.3. Synthesis of the iron-oxide folate conjugate:

Iron oxide nanoparticles were modified with folic acid. A solution of folic acid (2.5 mM) in 5 mL of dichloromethane (DCM) was prepared. Then, the FA solution was sonicated during 30 minutes. The resulting solution was then mixed with an ethanolic solution of *N*-(3-Dimethylaminopropyl)-*N'*-ethylcarbodiimide (EDC) (75 mM) and 4-(dimethylamino) pyridine (DMAP) (15 mM). Afterwards, the solution was sonicated using a high-intensity ultrasound probe during 2 h (see figure 1b). The solution was allowed to stand overnight. Posteriorly, the solution was stirred vigorously at 25°C during 24 h, and the MNPs were recovered and washed *via* magnetic decantation, using ethanol and deionized water as diluents. The product was stored for use in the subsequent steps.

3.4. Synthesis of amine-functionalized magneto-fluorescent nanoparticles:

To functionalize the surface-modified nanoparticles with rhodamine B isothiocyanate (RITC), an aqueous suspension of 2-AEP-functionalized INOPs (~25 mg) was prepared and homogenized using a high-intensity ultrasound probe for 10 min. Then, RITC (0.25 mM) was dissolved in 10 mL of DMSO, and the solution of RITC was added dropwise to the aqueous suspension. Once the mixture was complete, the resulting suspension was sonicated for an hour in the dark. Particles were recovered by magnetic concentration and washed thoroughly with deionized water, samples were stored for posterior use.

3.5. Synthesis of iron oxide-folate-fluorescent nanoparticles:

To create the multifunctional system, ~1.3 mg of RITC (0.25 mM) was dissolved in 10 mL of DMSO. Then, the solution was added dropwise in the dark to the previous iron-oxide folate suspension (FA-IONPs). The resulting suspension was sonicated during an hour. After that, the system was thoroughly washed with deionized water *via* magnetic concentration, and stored for posterior use (see figure 1c).

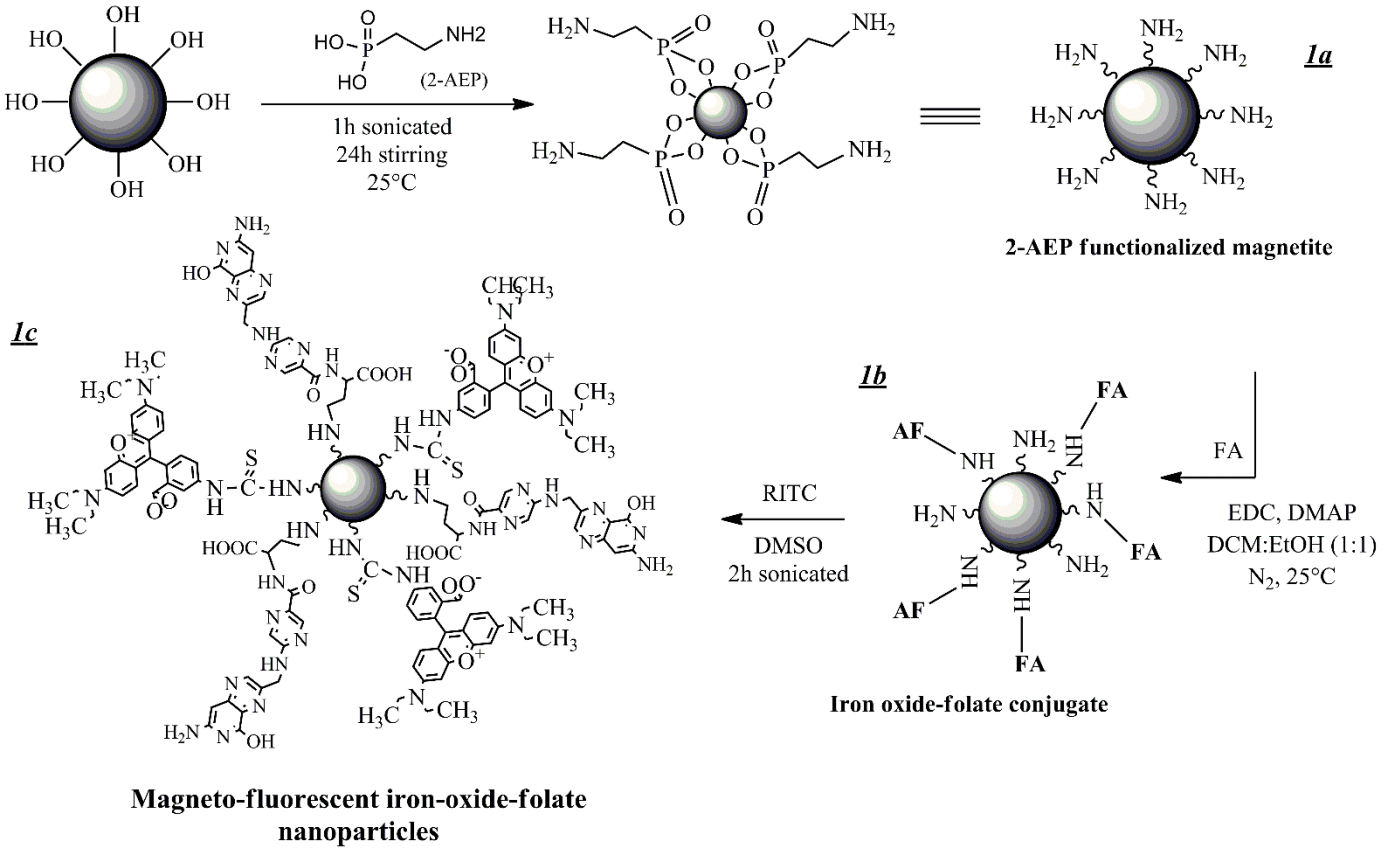

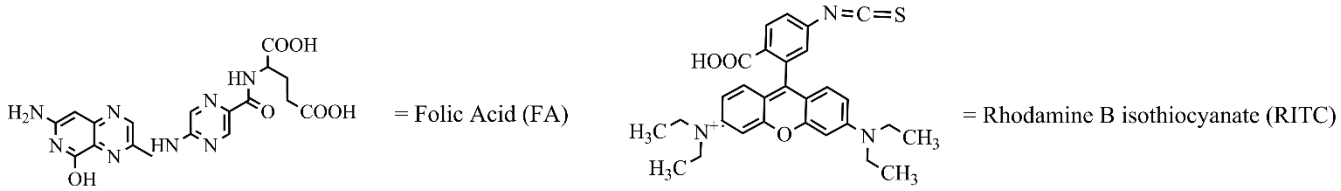

Figure 1. Schematic synthesis of amine-functionalized magnetite nanoparticles: a) the surface of IONPs was modified with 2-AEP to form an amine-functionalized phosphonate monolayer, b) folic acid/ rhodamine isothiocyanate were conjugated through the carbodiimide reaction, in order to obtain FA-IONPs-RITC.

4. RESULTS AND DISCUSSIONS:

4.1 Synthesis of magnetite and amino-functionalized nanoparticles:

Magnetite nanoparticles were successfully prepared by a chemical co-precipitation method in a basic medium, in accordance with the methods reported by different authors [27, 29, 57-59], with minor modifications. By this method, uniform particles are usually obtained [26].

The global chemical reaction of Fe_3O_4 precipitation is given by the overall reaction written as follow in Eq. (1) [5, 26]:

$$Fe^{2+} + 2Fe^{3+} + 8OH^- \rightarrow Fe_3O_4 + 4H_2O \qquad \text{Eq. (1)}$$

According to this reaction, a complete precipitation of Fe_3O_4 should be expected between pH 9 to 14, while maintaining a molar ratio of Fe^{3+}: Fe^{2+} of 2:1, and following the mechanism of Ostwald ripening growth [2, 5, 26]. With the synthesis route employed in this work at pH >13 and the same molar ratio, the magnetite nanoparticles exhibited optimal features.

The amino-modified nanoparticles used as precursor for the functionalization (due to the presence of terminal -NH_2 groups) were prepared using a derivative of phosphonic acid that undergoes easy formation of a self-assembled, strongly-organic monolayer on the surface of the nanoparticle, as has been previously established, by chemisorption of 2-AEP on INOPs for the introduction of polar functional groups onto the surface [2-3, 29, 44, 58, 60].

This coating allows further functionalization by chemical reactions [3]. Several studies have reported that phosphonates and phosphates bind efficiently to the iron oxide nanoparticle surface and can be useful as potential alternatives to fatty acids or other coatings. Also, they have good biocompability, a high capacity to form strong complexes with transition metals in aqueous solution, and show suitable affinity for the metal oxide surface [3, 60].

Considering that colloidal stability in an aqueous and physiological medium is one of the most important issues relating to the biomedical applications of nanoparticles [5, 21], these polar functional groups render nanoparticles thermodynamically stable against aggregation and keep them well-dispersed in aqueous media [5, 29, 44].

4.2. Surface modification of nanoparticles with rhodamine B isothiocyanate:

The formation of magneto-fluorescent nanoparticles was achieved through a covalent immobilization of rhodamine B isothiocyanate (RITC) on the particle surface, by means of a thiourea linkage through a nucleophilic addition of surface-pendent amine to isothiocyanate groups, to which primary amino groups of suitable organic molecules can be covalently linked, forming the magnetic fluorescent carrier, in this particular case [29-30, 58]. This system facilitates conjugation with a variety of small molecules through sulfhydryl, carboxyl, anhydride or imine chemistry, allowing easy manipulation of the surface functionality [29].

4.3. Surface modification of nanoparticles with folic acid:

To achieve specificity and enhanced efficacy, the magnetite nanoparticles were functionalized with folic acid [61]. The active-NH_2 groups present on the amino-functionalized nanoparticle surface were covalently conjugated with FA *via* non-selective activation of the carboxyl groups in its glutamic acid moiety by the carbodiimide method.

This method may lead to the formation of two structural isomers, in which FA is linked either through the α-carboxyl or γ-carboxyl group of its glutamic acid moiety. However, the folate linked *via* γ-carboxyl group is formed as the major isomer because is more prone to this reaction due to its higher reactivity and retains a strong affinity towards its receptor, whereas its α-carboxyl derivatives are not recognized as readily [44-58].

The aim of functionalization is to have systems with high specificity towards cancer cells, employing lower concentrations in order to minimize side effects, accompanied by an enhanced retention effect due to the poor lymphatic drainage [13, 23].

4.4. *Size and morphology:*

The co-precipitation method for obtaining IONPs is one of the fastest and easiest methods for this purpose. Nanoparticles were synthetized in a molar ratio of Fe^{3+}: Fe^{2+} of 2:1. Transmission electron microscopy (TEM) studies of IONPs revealed that the as-synthesized magnetite nanoparticles were closer to a spherical form, and were uniform and homogeneous, which corresponds to that previously reported [12, 14, 26, 57].

The IONPs were obtained with a mean hydrodynamic diameter of 18.65 nm ± 0.178 nm (figure 2a). Size-distribution showed a monomodal population. The frequency histogram is shown in figure 2b.

According to previous reports, a size between 10-100 nm results in systems with a size small enough to avoid the mononuclear phagocyte system (MPS) and to penetrate the capillary body cavities. Also, for medical applications, nanoparticles must conform to a size smaller than 100 nm, at which they possess unique physicochemical and non-toxic characteristics, and biocompatibility [13-14, 31, 41, 62].

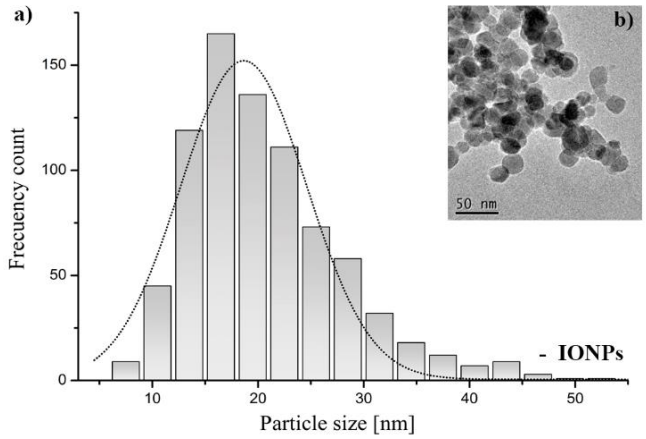

Figure 2. a) Particle size distribution (PSD) histogram of unmodified magnetite nanoparticles and b) TEM micrograph of the same system.

4.5. Surface chemistry:

4.5.1. FT-IR studies:

In figure 3a, the transmission spectra of unmodified and amine-functionalized magnetite nanoparticles have been depicted and figure 3b is the spectra of iron oxide-folate conjugate nanoparticles (4000-400 cm^{-1}). The transmission far-infrared spectra of unmodified magnetite nanoparticles (700-40 cm^{-1}) is reported in figure 3c.

a) Magnetite nanoparticles: The FT-IR spectra obtained both in the far and the medium zone showed the characteristic vibrations for the iron oxide material, in its magnetite phase. For the first case, (700-40 cm^{-1}), the medium-intense band at 345 cm^{-1} is attributed to the vibration of the magnetite core. Said band has been previously reported to be specific for Fe_3O_4 [63-64]. In the second case, for the medium zone, (4500-400 cm^{-1}), the expected vibrational bands were

observed at 558 cm^{-1} and 3256 cm^{-1}. The first one corresponds to the specific Fe-O vibration of iron oxide nanoparticles [8, 14, 21, 29, 31, 44, 58, 63, 65-68], which confirms the material expected. The band at 3256 cm^{-1} was assigned to the -OH *st* vibration groups due to adsorbed water on the surface of the iron oxide nanoparticles [8, 14, 29, 63, 66-67].

b) Amino-modified nanoparticles: In the 2-AEP functionalized IONPs, in the medium zone, the strong band at 1026 cm^{-1} showed that the compound was adsorbed onto the magnetite surface and is from the *st* vibration related to the overlapping of the signals which correspond to the vibrations of M-O-P, P=O and the P-O bond [29, 44, 58, 60, 69]. The band at 3361 cm^{-1} corresponds to the -NH_2 group *st* vibration, which is confirmed with the bending scissoring vibration present at 1631 cm^{-1}. These two bands confirm the presence of the amino-terminal groups on the nanoparticle surface, which are necessary for the posterior functionalization [29, 58, 65, 69]. The peak for the magnetite core at 558 cm^{-1} shifts towards higher wavenumbers, to 570 cm^{-1}. Also, a significant decrease in the intensity of this band is observed, which indicates the adsorption of phosphonic acids onto the magnetite surface. The presence of this band suggests that the modification does not alter the nanoparticle's properties [29, 58, 63, 65].

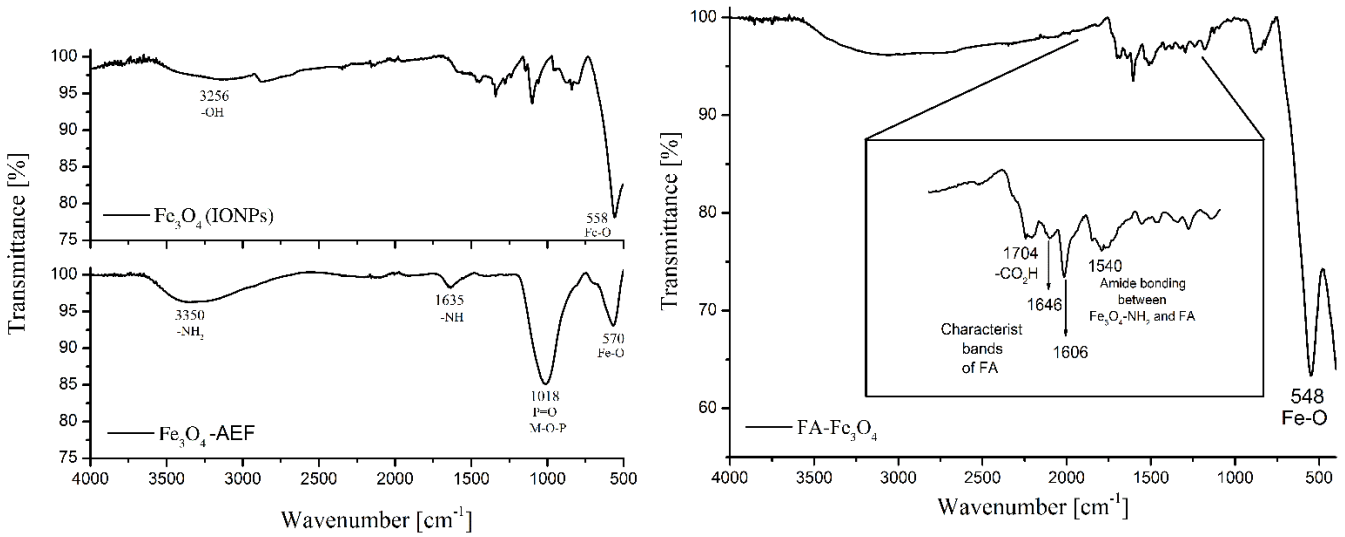

Figure 3. FT-IR spectra of a) unmodified and amino-functionalized magnetite nanoparticles, b) iron oxide-folate conjugate nanoparticles, and c) unmodified magnetite nanoparticles in far infrared.

c) Fe_3O_4/FA system: In the FT-IR spectrum of folate-conjugated nanoparticles, the peak in the range of 3100- 3500 cm^{-1} was assigned to the N-H *st* vibration from the -NH_2 and amine NH groups from folic acid. At 1648 cm^{-1}, the band present is related to the carbonyl group *st* vibration from amide and acidic groups, which exhibits less intensity and was shifted to ~1700 cm^{-1}, indicating that folic acid was successfully attached to the IONPs [31, 39, 58, 65].

The bands at 1606 cm^{-1} and 1548 cm^{-1} were assigned to the characteristic FA *st* vibrations (amide II and amide I, respectively), which indicate the successful conjugation to the nanoparticle surface [29, 39, 44, 58, 70]. The presence of the new band at 1530 cm^{-1} was confirmed from the *st* vibration of the amide binding between Fe_3O_4-NH_2-FA, which indicates the formation of an extra amide bond attributed to the FA attachment onto the surface of IONPs, as well as the amide bands within the FA structure [29].

Finally, it is important to mention that the vibration from the magnetite core still appears at 548 cm^{-1}, which suggests that even with the formation of the conjugate, the core does not suffer any important alteration [39].

4.5.2. Raman studies:

In figure 4, the Raman spectra from the unmodified magnetite, folic acid conjugate, rhodamine conjugate and folic acid/rhodamine magnetite nanoparticles have been depicted.

The Fe_3O_4-FA Raman spectra (1800-200 cm^{-1}) showed medium-intensity Raman bands at 1160 cm^{-1}, due to the C=N *rocking* vibration of the pteridine ring, and at 674 cm^{-1}, from the *asymmetric stretching* vibration of the C=C bond from the *p*-amino benzoic acid. Also, in this wavenumber, the *stretching symmetric* vibration from the C=N in the amide bond within the system and from the pteridine ring, are present. Additionally, the band related to the magnetite is shown at 326 cm^{-1}. In the case of the bare magnetite nanoparticles, only the band at 327 cm^{-1}, which is attributed to this specific material, appears.

For the IONPs/rhodamine isothiocyanate system, an *asymmetric stretching* vibration at 1435 cm^{-1}, corresponding to the xanthene group of rhodamine, is present, the corresponding band from magnetite.

Finally, the multifunctional system presents medium-intensity Raman bands corresponding to *asymmetric stretching* vibration of the C=C group at 674 cm^{-1} from the xanthene group and from the unsaturations of the folic acid. At this same wavenumber, the *symmetric stretching* vibration of the C=N bond from the amide binding in the system, is present. Also, is evident the vibration from Fe-O (magnetite) in the same wavenumber as bare magnetite at 326 cm^{-1}. The strong band at ~ 1489 cm^{-1} in all the systems could be from a specific vibration of the magnetite material.

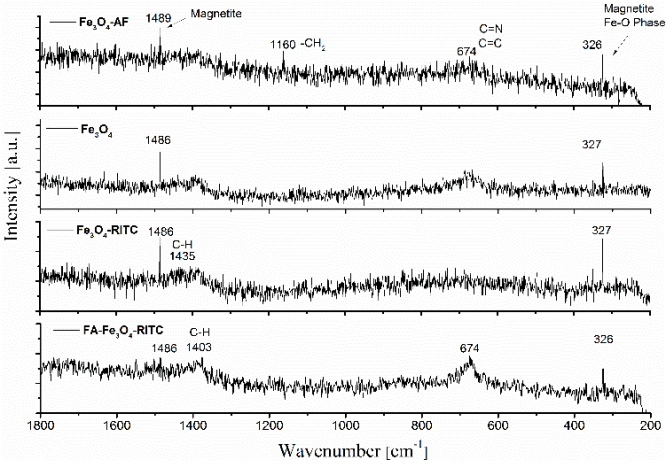

Figure 4. Raman spectra of different systems: magnetite-folic acid, bare magnetite, magnetite-rhodamine isothiocyanate and IONPs-folic acid/ rhodamine isothiocyanate, from 1800- 200 cm^{-1}.

4.5.3. UV-Vis studies:

UV-Vis studies: In figure 5, the UV-Vis spectra from the unmodified magnetite, folic acid conjugate, rhodamine conjugate, folic acid/rhodamine magnetite nanoparticles, folic acid solution and rhodamine solution have been depicted.

The magnetite core of the system, in the range 200-700 nm of the UV-Vis spectra, showed a characteristic band around 360 nm which demonstrated a suitable synthesis. The peak at ~280 nm was assigned to FA due to the well-known π- π* transitions from the pteridine ring moiety in the FA structure [70].

This UV-Vis band is present in the FA aqueous solution at 282 nm, and in the Fe_3O_4-FA system at 283 nm. In the case of the Fe_3O_4-AF-RITC system, in which FA is also present, the band still appeared at 283 nm [39, 66].

On the other hand, the UV-Vis spectra for the same systems but focus on the RITC molecules, a band around 550 nm is present, which has been reported in previous works (536 nm for Fe_3O_4-RITC and 580 nm for Fe_3O_4-AF-RITC) [10, 71], and although it is broad, the maximum absorption occurs in the same region. The analytical information obtained with this technique suggests that the conjugation of the FA at the surface of the IONPs was carried out successfully, in good agreement with the FT-IR study. Based on these results, it is possible to suggest that the conjugation of FE_3O_4-RITC was successfully carried out, as well as the preparation of the multifunctional system FE_3O_4-AF-RITC.

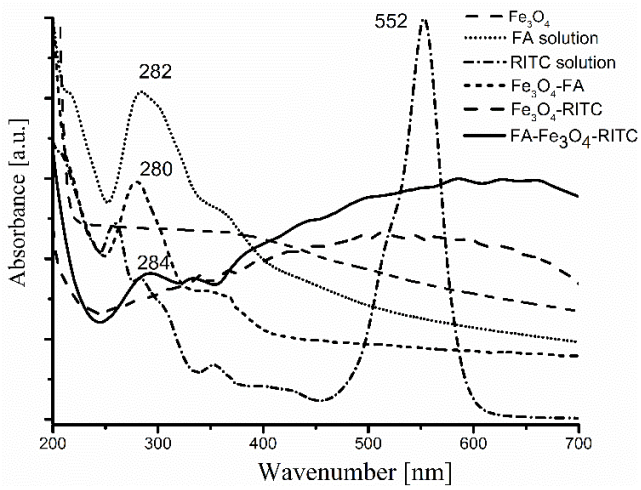

Figure 5. UV-Vis spectra of unmodified magnetite, folic acid conjugate, rhodamine conjugate, folic acid/rhodamine magnetite nanoparticles, folic acid solution and rhodamine solution.

4.5.4. Fluorescence studies:

In figure 6, the fluorescence emission spectra from magnetite, folic acid conjugate, rhodamine conjugate, folic acid/rhodamine magnetite nanoparticles, folic acid solution and rhodamine solution have been depicted.

The band around 575 nm for the fluorescent emission spectra of the systems containing rhodamine (FA-Fe_3O_4-RITC and Fe_3O_4-RITC) and the one for the solution of RITC are in excellent agreement with the previously reported around 570- 575 nm [30, 33, 72-73]. The differences in the band are due to the chemical environment, and the low intensity is due to the quantity employed in the synthesis procedure (being less than 0.1 % of the total system).

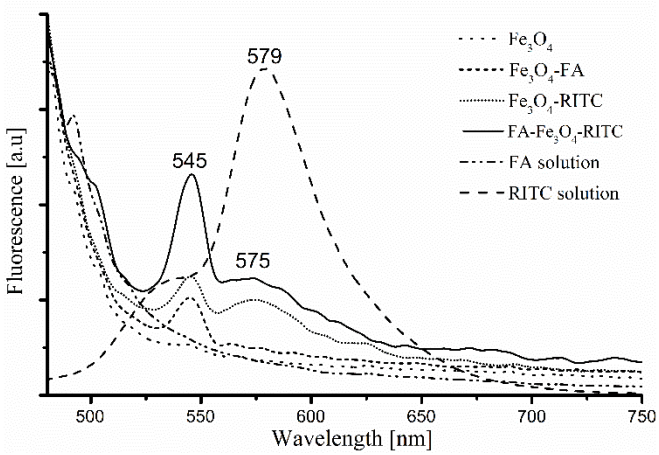

Figure 6: Fluorescence emission spectra of magnetite, folic acid conjugate, rhodamine conjugate, folic acid/rhodamine magnetite nanoparticles, folic acid solution and rhodamine solution.

For the systems with FA, either FA-Fe_3O_4-RITC or FA-Fe_3O_4, the emission spectra presented a common band at 545 nm. In the case of FA-Fe_3O_4-RITC, a second band appeared at 579 nm, that corresponds to the RITC molecule previously described. For the band at 545 nm, according to previous studies, FA could be present in two forms (basic and acid), due to the pteridine ring moiety. In the emission spectra, the alkaline form used to have a band between 300-400 nm and another band in the 230-290 nm range with higher absorption coefficients that their acid form. On the other hand, the complete molecule of FA usually presents two bands (at 255 nm and 285 nm) in its alkaline form, and an overlapping of the same for the acid form, resulting in a unique band at 285 nm.

Considering this and assuming that the system conjugation was carried out according to the previously proposed, it is possible to suggest that the pteridine moiety is exposed on system' surface. Thus, with the fluorescence studies, it was possible to observe a relative increment of the band at 545 nm, which corresponds to the alkaline form, indicating in that way, the correct and suitable system conjugation. However, the magnetite core presented a lower intensity band in the same region (~545 nm), so it is possible to suggest that in the FA-Fe_3O_4-RITC and Fe_3O_4-RITC systems, a contribution of both compounds (Fe_3O_4 and FA) existed in order to increase the intensity of the band in that wavelength. As for the Fe_3O_4-RITC system, there was no FA (with its pteridine ring moiety), which can cause the appearance of a band.

4.6. FA conjugated over the IONPs' surface:

In order to obtain the percentage of saturation, was necessary to measure both, the reaction supernatant and the resultant nanoparticle suspension, to confirm the quantity of FA successfully conjugated.

According to the results obtained, was necessary to dilute the concentration of FA-Fe_3O_4 suspension until reached an adequate concentration to the standard curve, so as not to exceed the sensitivity of the instrument.

In accordance to the percentages obtained from the different systems was possible to observe that even at the lowest initial concentration of FA, a >95% of FA in IONPs surface was reached. Also was important the fact that the reaction had a maximal saturation point with a concentration > 5.0 mM, where the percentages were over 98%. These data resulted important to optimize the quantities of FA in the final system. In table 1, the concentrations of FA employed and the percentage of conjugation over the nanoparticle surface are shown.

Table 1. Determination of concentration of FA conjugated over the IONPs' surface

Initial [FA] (mM)	% FA in IONPs' surface (%)	Initial [FA] (mg mL^{-1})	[FA] in IONPs' surface (mg mL^{-1})
10.0	98.84	4.4	4.35
8.8	98.33	3.8	3.74
7.5	98.20	3.2	3.14
6.3	98.03	2.6	2.55
5.0	97.79	2.2	2.15
2.5	96.08	1.0	0.96

4.7. Determination of the RITC concentration on the IONPs' surface:

The establishment of the percentage of saturation, was measured both, the reaction supernatant and the resultant nanoparticle suspension in order to obtain the quantity of RITC conjugated in the magemite nanoparticle. In this specific case, due to the concentrations of RITC used (too small to the detection limit), the data of the supernatants were employed to calculate the final concentration over the NPs surface.

In accordance to the results obtained, was necessary to dilute the concentration of the supernatant solution until reached an adequate concentration to the standard curve, so as not to exceed the sensitivity of the instrument. With the results of the percentages obtained from the different systems was possible to observe that even at the lowest initial concentration of RITC, a >95% of this compound in IONPs surface was possible. The saturation of the system for this specific case was reached even with the lowest initial concentration employed, where the percentages were over 96%.

These data resulted important to optimize the quantities of RITC in the final system. In the table 2 the RITC concentrations and the conjugation percentage are shown.

Table 2. Determination of RITC concentration conjugated on the IONPs' surface

Initial [RITC] (mM)	% RITC in IONPs' surface (%)	Initial [RITC] (mg mL^{-1})	[RITC] in IONPs' surface (mg mL^{-1})
0.0125	96.80	0.75	0.726
0.0375	96.96	2.25	2.1816
0.0625	97.00	3.75	3.6375

Finally, was evident that there was not necessary a large amount of reactants (FA and RITC) to achieve a suitable conjugation of both systems. Besides the profits of the system allows the optimization of the same, in order to fit the concentration of RITC that could be sufficient enough for optical image by FI and the concentration of FA which enables a good targeting of the system.

4.8. Nanoparticle-induced cytotoxicity:

For the cell viability test, the IONPs exposure time was 24 h as usually. It is important to note that the highest IONPs concentration employed (0.5 mg mL^{-1}) was lower than concentrations used in other studies with different cell lines, but much higher than in many other works with that employed magnetite [49].

In order to corroborate the system biocompatibility, the FA-Fe_3O_4-RITC NPs (0.5 mg mL^{-1}, 0.25 mg mL^{-1}, 0.125 mg mL^{-1}, 0.0625 mg mL^{-1} and 0.0 mg mL^{-1}) were incubated during 24 h in HeLa cells, in a humidified 5%-CO_2/95%-air atmosphere. After treatment, the cells were evaluated using a crystal violet staining.

According to the results shown in figure 7, there was a significant difference between the lowest (0.0 mg mL^{-1}) and the highest (0.5 mg mL^{-1}) concentrations. Despite this, all treatments showed cell viability higher than 80%. The highest FA-Fe_3O_4-RITC concentration (0.5 mg mL^{-1}) showed 82.5% of viability, which demonstrated the FA-Fe_3O_4-RITC biocompatibility.

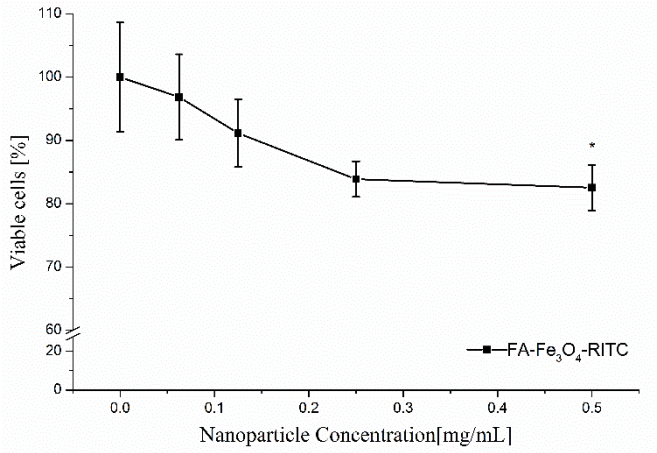

Figure 7. Effect of folate-rhodamine-conjugated nanoparticles on the HeLa cells viability. Cells incubated with different nanoparticle concentrations for 24 h at 37°C followed by crystal violet staining. No significant reduction in cellular viability was observed, the survival rate being higher than 80%, even at the highest nanoparticle concentration.

4.9. Cellular uptake:

Generally, once a tumor- targeting ligand conjugate has reached its target receptor, uptake and internalization can occur through receptor-mediated bio-events, mainly receptor-mediated endocytosis, but phagocytosis and pinocytosis can also contribute to internalization. After endocytosis, most but not all ligand-receptor complexes dissociate in the endosomes and the ligand eventually ends up in the lysosomes, while receptors are often recycled and transported back to the cell surface by transport vesicles [70].

The results of the internalization of MNPs are dependent on two factors: I) the type of MNPs coating, and II) The MNPs concentration [49]. In the system designed, FA demonstrated that it can promote tumor cell receptor-mediated internalization [35].

As was predicted from the cytotoxicity experiments, photomicrographs (taken with an Olympus IX80 inverted confocal microscope and an AxioVision software) clearly showed that cellular structures were well preserved without morphology abnormalities after nanoparticles treatment (see figure 8).

The folate-conjugated nanoparticles were found to be distributed within the cytoplasm, suggesting cellular internalization through receptor-mediated endocytosis, instead of adhesion to the cell surface. This study unequivocally establishes that all the iron-oxide folate nanoconjugates, developed in the course of this research, are preferentially targeted towards cancer cells and effectively internalized (63 % of internalization with respect to 53 % of the blocked group). Also, the results indicated that the system with FA could enhanced the intracellular uptake of the IONPs effectively, assuming that FA works as a tumor-targeting ligand, which likely enhances receptor mediated endocytosis [70]. Receptor-mediated internalization of nanoparticles by FA receptor in overexpressing cancer cells was further demonstrated using an inverted confocal microscope (Olympus IX80).

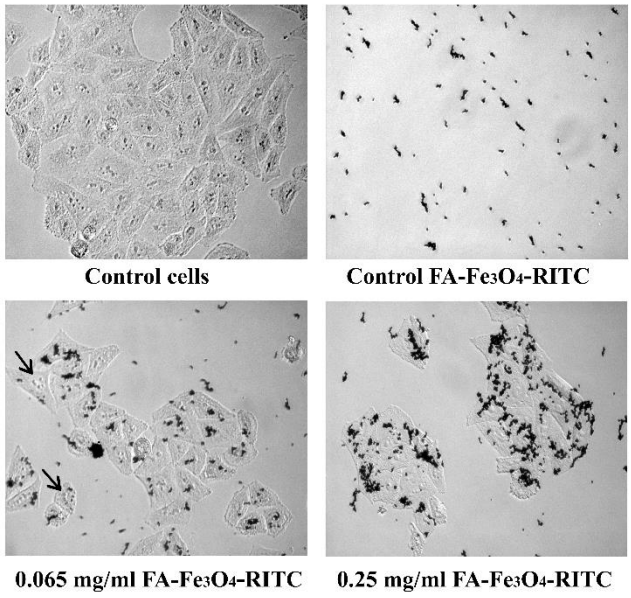

Figure 8. Photomicrographs of cellular uptake test in HeLa cells at two different concentrations. The black arrows show the internalization of the system, which is visible even at low concentrations (0.065 mg mL^{-1}).

5. CONCLUSIONS

In this work, iron oxide magnetite nanoparticles, modified with folic acid/ rhodamine were successfully synthetized *via* carbodiimide reaction. This system demonstrated optimal conditions for their use in medical application. The proposed uptake mechanism is through folic acid receptor endocytosis. However, to assure that such mechanism is involved, it is necessary to carry out studies focused on the labeling and tracing of the mechanism through recognition of its receptor. Also, PK studies are crucial in order to elucidate their behavior *in vivo*, and also to prove their magnetic and fluorescent properties.

CONFLICT OF INTEREST

The authors confirm that this article content has no conflict of interest.

ACKNOWLEDGEMENTS

This study was supported by the International Atomic Energy Agency (CRP-F22064, Contract No. 18358) and the Universidad Autónoma del Estado de México, through the project No. 3543/2013CHT.

REFERENCES

[1] Chen, K. and Chen X., Design and Development of Molecular Imaging Probes. Curr Top Med Chem, 2010. 10(12): p. 1227-1236.

[2] Wu, W., Q. He, and C. Jiang, Magnetic iron oxide nanoparticles: synthesis and surface functionalization strategies. Nanoscale Res Lett, 2008. 3(11): p. 397-415.

[3] Mahmoudi, M., *et al.*, Superparamagnetic iron oxide nanoparticles: promises for diagnosis and treatment of multiple sclerosis. ACS Chem Neurosci, 2011. 2(3): p. 118-40.

[4] Dongwon Y., Jae-Hyun L., Tae-Hyun S. and Cheon J., Theranostic Magnetic Nanoparticles. Accounts of Chemical Research, 2011. 44(10): p. 863-874.

[5] Gupta, A.K. and Gupta M., Synthesis and surface engineering of iron oxide nanoparticles for biomedical applications. Biomaterials, 2005. 26(18): p. 3995-4021.

[6] Zeinali Sehrig, F., *et al*., An update on clinical applications of magnetic nanoparticles for increasing the resolution of magnetic resonance imaging. Artif Cells Nanomed Biotechnol, 2015: p. 1-6.

[7] Yu K.M., Park J., and Jon S., Targeting strategies for multifunctional nanoparticles in cancer imaging and therapy. Theranostics, 2012. 2(1): p. 3-44.

[8] Rahman M.M., Khan S.B. *et al.*, Detection of a prepitant drug based on low-dimensional un-doped iron oxide nanoparticles prepared by a solution method. Electrochimica Acta, 2012. 75: p. 164-170.

[9] Hola, K., *et al*., Tailored functionalization of iron oxide nanoparticles for MRI, drug delivery, magnetic separation and immobilization of biosubstances. Biotechnol Adv, 2015. 33(6 Pt 2): p. 1162-76.

[10] Thuy T.T. Guyen, H.T.T.D., Johan Basuki, Véronique Montembault, *et.al.*, Functional Iron Oxide Magnetic Nanoparticles with Hyperthermia-Induced Drug Release Ability by Using a Combination of Orthogonal Click Reactions. Angewandte Communications, 2013. 52(52): p. 14152-14156.

[11] Schweiger, C., *et al.*, Novel magnetic iron oxide nanoparticles coated with poly(ethylene imine)-g-poly(ethylene glycol) for potential biomedical application: synthesis, stability, cytotoxicity and MR imaging. Int J Pharm, 2011. 408(1-2): p. 130-7.

[12] Klein, S., *et al.*, Superparamagnetic iron oxide nanoparticles as radiosensitizer *via* enhanced reactive oxygen species formation. Biochem Biophys Res Commun, 2012. 425(2): p. 393-7.

[13] Mahmoudi, M., *et al.*, Superparamagnetic iron oxide nanoparticles (SPIONs): development, surface modification and applications in chemotherapy. Adv Drug Deliv Rev, 2011. 63(1-2): p. 24-46.

[14] Easo, S.L. and P.V. Mohanan, Dextran stabilized iron oxide nanoparticles: synthesis, characterization and *in vitro* studies. Carbohydr Polym, 2013. 92(1): p. 726-32.

[15] Jang, B., *et al.*, Dual delivery of biological therapeutics for multimodal and synergistic cancer therapies. Adv Drug Deliv Rev, 2016. 98: p. 113-33.

[16] Erathodiyil N. and Ying J., Functionalization of inorganic nanoparticles for bioimaging applications. Accounts of chemical research, 2011. 44(10): p. 925-935.

[17] Choi, K.Y., *et al*., Theranostic nanoplatforms for simultaneous cancer imaging and therapy: current approaches and future perspectives. Nanoscale, 2012. 4(2): p. 330-42.

[18] Rosen, J.E., *et al.*, Iron oxide nanoparticles for targeted cancer imaging and diagnostics. Nanomedicine, 2012. 8(3): p. 275-90.

[19] Rümenapp, C., *et al.*, Detection of molecules and cells using nuclear magnetic resonance with magnetic nanoparticles. Journal of Magnetism and Magnetic Materials, 2015. 380: p. 271-275.

[20] Laurent, S., *et al.*, Magnetic fluid hyperthermia: focus on superparamagnetic iron oxide nanoparticles. Adv Colloid Interface Sci, 2011. 166(1-2): p. 8-23.

[21] Barick, K.C., *et al.*, Carboxyl decorated Fe_3O_4 nanoparticles for MRI diagnosis and localized hyperthermia. J Colloid Interface Sci, 2014. 418: p. 120-5.

[22] Zhou, X., *et al.*, Multifunctional fluorescent magnetic nanoparticles for lung cancer stem cells research. Colloids Surf B Biointerfaces, 2015. 134: p. 431-9.

[23] Figuerola, A., *et al*., From iron oxide nanoparticles towards advanced iron-based inorganic materials designed for biomedical applications. Pharmacol Res, 2010. 62(2): p. 126-43.

[24] Bennett, K.M., *et al*., MR imaging techniques for nano-pathophysiology and theranostics. Adv Drug Deliv Rev, 2014. 74: p. 75-94.

[25] Kumar, C.S. and Mohammad F., Magnetic nanomaterials for hyperthermia-based therapy and controlled drug delivery. Adv Drug Deliv Rev, 2011. 63(9): p. 789-808.

[26] Lodhia, J., *et al.*, Development and use of iron oxide nanoparticles (Part 1): Synthesis of iron oxide nanoparticles for MRI. Biomed Imaging Interv J, 2010. 6(2): p. e12.

[27] Iwasaki, T., Novel mechanochemical process for aqueous phase synthesis of superparamagnetic magnetite nanoparticles, in Materials Science and Technology, S.D. Hutagalung, Editor. 2012, InTech: Japan. p. 235-256.

[28] Kristen K., Comfort E.I.M., Laura K., Brayadich-Stolle and Saber M., Interference of silver, gold, and iron oxide nanoparticles of epidermal growth factor signal transduction in epithelial cells. American Chemical Society Nano, 2011. 5(12): p. 1000-1008.

[29] Das, M., *et al.*, Bio-functionalization of magnetite nanoparticles using an aminophosphonic acid coupling agent: new, ultradispersed, iron-oxide folate nanoconjugates for cancer-specific targeting. Nanotechnology, 2008. 19(41): p. 415101.

[30] Magro M., *et al.*, Charge binding of rhodamine derivative to OH-stabilized nanomaghemite: universal nanocarrier for construction of magnetofluorescent biosensors. Acta Biomater, 2012. 8(6): p. 2068-76.

[31] Thu Huong L.T., Hoai Nam H., Doan H. D., *et. al.*, Folate attached, curcumin loaded Fe_3O_4 nanoparticles: A novel multifunctional drug delivery system for cancer treatment. Materials Chemistry and Physics, 2016. 172: p. 98-104.

[32] Fan, Z., *et al.*, Theranostic nanomedicine for cancer detection and treatment. J Food Drug Anal, 2014. 22(1): p. 3-17.

[33] Song, C., Wang G.Y. and Kong D.M., A facile fluorescence method for versatile biomolecular detection based on pristine alpha-Fe_2O_3 nanoparticle-induced fluorescence quenching. Biosens Bioelectron, 2015. 68: p. 239-44.

[34] Castillo, J.J., *et al.*, Adsorption and Vibrational Study of Folic Acid on Gold Nanopillar Structures Using Surface-enhanced Raman Scattering Spectroscopy. Nanomaterials and Nanotechnology, 2015: p. 1.

[35] Scomparin, A., *et al.*, A comparative study of folate receptor-targeted doxorubicin delivery systems: Dosing regimens and therapeutic index. J Control Release, 2015. 208: p. 106-20.

[36] Lu, Y. and Low P.S., Folate-mediated delivery of macromolecular anticancer therapeutics agents. Adv Drug Deliv Rev, 2002. 54: p. 675-693.

[37] Chen, C., *et al.*, Structural basis for molecular recognition of folic acid by folate receptors. Nature, 2013. 500(7463): p. 486-9.

[38] Parker, N., *et al.*, Folate receptor expression in carcinomas and normal tissues determined by a quantitative radioligand binding assay. Anal Biochem, 2005. 338(2): p. 284-93.

[39] Krais, A., *et al.*, Targeted uptake of folic acid-functionalized iron oxide nanoparticles by ovarian cancer cells in the presence but not in the absence of serum. Nanomedicine, 2014. 10(7): p. 1421-31.

[40] Sudimack J. and Lee J.R., Targeted drug delivery via the folate receptor. Advanced Drug Delivery Reviews, 2000. 41: p. 147-162.

[41] Nyström A.M. and Wooley K.L., The importance of chemistry in creating well-defined nanoscopic embedded therapeutics: Devices capable of the dual functions of imaging and therapy. Accounts of Chemical Research, 2011. 44(10): p. 969-978.

[42] Wen, J., *et al.*, Apoptosis selectively induced in BEL-7402 cells by folic acid-modified magnetic nanoparticles combined with 100 Hz magnetic field. Int J Nanomedicine, 2014. 9: p. 2043-50.

[43] Kelemen, L.E., The role of folate receptor alpha in cancer development, progression and treatment: cause, consequence or innocent bystander? Int J Cancer, 2006. 119(2): p. 243-50.

[44] Mohapatra, S., *et al.*, Synthesis of highly stable folic acid conjugated magnetite nanoparticles for targeting cancer cells. Nanotechnology, 2007. 18(38): p. 385102.

[45] Beija, M., *et. al.*, Synthesis and applications of Rhodamine derivatives as fluorescent probes. Chem Soc Rev, 2009. 38(8): p. 2410-33.

[46] Bakkialakshmi, S., Selvarani P., and Chenthamarai S., Fluorescence quenching of Rhodamine B base by two amines. Spectrochim Acta A Mol Biomol Spectrosc, 2013. 105: p. 557-62.

[47] Natarajan, A., *et al.*, Synthesis, chemical reactivity, and photophysical properties of 2′,7′-phenylated rhodamine dyes. Tetrahedron Letters, 2014. 55(30): p. 4222-4226.

[48] Janib, S.M., Moses A.S. and MacKay J.A., Imaging and drug delivery using theranostic nanoparticles. Adv Drug Deliv Rev, 2010. 62(11): p. 1052-63.

[49] Calero, M., *et al.*, Efficient and safe internalization of magnetic iron oxide nanoparticles: two fundamental requirements for biomedical applications. Nanomedicine, 2014. 10(4): p. 733-43.

[50] Luo, S., *et al.*, A review of NIR dyes in cancer targeting and imaging. Biomaterials, 2011. 32(29): p. 7127-38.

[51] Pauli, J., *et al.*, Novel fluorophores as building blocks for optical probes for in vivo near infrared fluorescence (NIRF) imaging. J Fluoresc, 2010. 20(3): p. 681-93.

[52] Shi, D., Bedford N.M. and Cho H.S., Engineered multifunctional nanocarriers for cancer diagnosis and therapeutics. Small, 2011. 7(18): p. 2549-67.

[53] Rao, J., Dragulescu-Andrasi A., and Yao H., Fluorescence imaging *in vivo*: recent advances. Curr Opin Biotechnol, 2007. 18(1): p. 17-25.

[54] Jarzebski, M., *et al.*, Core–shell fluorinated methacrylate nanoparticles with Rhodamine-B for confocal microscopy and fluorescence correlation spectroscopy applications. Journal of Fluorine Chemistry, 2016. 183: p. 92-99.

[55] Strijkers G., Mulder W., Van Tilborg G. and Nicolay K., MRI contrast agents: current status and future perspectives. Anti-Cancer Agents in Medicinal Chemistry, 2007. 7(3): p. 291-305.

[56] Lopez-Cebral, R., *et al.*, Progress in the characterization of bio-functionalized nanoparticles using NMR methods and their applications as MRI contrast agents. Prog Nucl Magn Reson Spectrosc, 2014. 79: p. 1-13.

[57] Banerji, B., *et al.*, Synthesis, characterization and cytotoxicity study of magnetic (Fe_3O_4) nanoparticles and their drug conjugate. RSC Advances, 2012. 2(6): p. 2493.

[58] Das, M., *et al.*, "Clickable", trifunctional magnetite nanoparticles and their chemoselective biofunctionalization. Bioconjug Chem, 2011. 22(6): p. 1181-93.

[59] Zhang, C., *et al.*, Specific targeting of tumor angiogenesis by RGD-conjugated ultrasmall superparamagnetic iron oxide particles using a clinical 1.5-T magnetic resonance scanner. Cancer Res, 2007. 67(4): p. 1555-62.

[60] Mohapatra, S. and Pramanik P., Synthesis and stability of functionalized iron oxide nanoparticles using organophosphorus coupling agents. Colloids and Surfaces A: Physicochemical and Engineering Aspects, 2009. 339(1-3): p. 35-42.

[61] Jabr-Milane, L., *et al.*, Multi-functional nanocarriers for targeted delivery of drugs and genes. J Control Release, 2008. 130(2): p. 121-8.

[62] Singh, A.K., Structure, Synthesis, and Application of Nanoparticles. 2016: p. 19-76.

[63] Sun, J., *et al.*, Synthesis and characterization of biocompatible Fe_3O_4 nanoparticles. J Biomed Mater Res A, 2007. 80(2): p. 333-41.

[64] Gotić M. and Musić S., Mössbauer, FT-IR and FE SEM investigation of iron oxides precipitated from $FeSO_4$ solutions. Journal of Molecular Structure, 2007. 834-836: p. 445-453.

[65] Cao, H., *et al.*, Fabrication of cyclodextrin-functionalized superparamagnetic Fe_3O_4/amino-silane core–shell nanoparticles *via* layer-by-layer method. Applied Surface Science, 2009. 255(18): p. 7974-7980.

[66] Karamipour, S., Sadjadi M.S., and Farhadyar N., Fabrication and spectroscopic studies of folic acid-conjugated Fe_3O_4@Au core-shell for targeted drug delivery application. Spectrochim Acta A Mol Biomol Spectrosc, 2015. 148: p. 146-55.

[67] Sitthichai, S., *et al.*, CMC-coated Fe_3O_4 nanoparticles as new MRI probes for hepatocellular carcinoma. Applied Surface Science, 2015. 356: p. 972-977.

[68] Yazdani, F., Fattahi B., andAzizi N., Synthesis of functionalized magnetite nanoparticles to use as liver targeting MRI contrast agent. Journal of Magnetism and Magnetic Materials, 2016. 406: p. 207-211.

[69] Pretsch, E., Bühlmann P., and Badertscher M., Structure determination of organic compounds: tables of spectral data. 4th ed. 2009, Verlag Berlin Heidelberg: Springer. 444.

[70] Zhao, L., *et al.*, Enhanced cellular uptake and phototoxicity of Verteporfin-conjugated gold nanoparticles as theranostic nanocarriers for targeted photodynamic therapy and imaging of cancers. Materials Science and Engineering: C, 2016. 67: p. 611-622.

[71] Kim, K., *et al.*, Rhodamine B isothiocyanate-modified Ag nanoaggregates on dielectric beads: a novel surface-enhanced Raman scattering and fluorescent imaging material. Biosens Bioelectron, 2009. 24(7): p. 1864-9.

[72] Pylaev, T.E., *et al.*, DNA detection assay based on fluorescence quenching of rhodamine B by gold nanoparticles: The optical mechanisms. Journal of Quantitative Spectroscopy and Radiative Transfer, 2013. 131: p. 34-42.

[73] Liu, H., *et al.*, Luminescent Rhodamine B doped core–shell silica nanoparticle labels for protein microarray detection. Dyes and Pigments, 2013. 98(1): p. 119-124.

CONCLUSIONES GENERALES

CONCLUSIONES Y PERSPECTIVAS

- De acuerdo a los resultados obtenidos para la síntesis de nanopartículas de óxido de hierro mediante una reacción de coprecipitación se ha observado y concluido que el valor de pH de las soluciones empleadas juega un papel muy importante para que estas no pierdan sus características además de sus propiedades magnéticas.
- El empleo de la técnica de coprecipitación resulta un modo fácil de obtener las nanopartículas deseadas de Fe_3O_4, además de que proporcionan poblaciones monodispersas.
- La modificación superficial de las nanopartículas de Fe_3O_4 con ácido 2-amino-etilfosfónico de acuerdo a los espectros vibracionales obtenidos en la región del infrarrojo medio muestran una adecuada conjugación por las bandas mostradas tanto en las nanopartículas sin recubrimiento, como en las ya tratadas, sin embargo, sería importante poder cuantificar o de una manera aproximada tener idea del porcentaje de unión de la densidad de moléculas de ácido 2-amino-etilfosfónico sobre la superficie de nanopartículas de Fe_3O_4.
- La reacción de carbodiimida planteada para la obtención del conjugado de vectorización Fe_30_4-AF, resultó en un método adecuado, para el cual, aún a concentraciones iniciales relativamente bajas de ácido fólico (>2.5 mM) se logró obtener un porcentaje de conjugación sobre la superficie de la nanopartícula mayor a 95%, pudiendo asegurar de esta manera que la vectorización sea mantenida.
- Las diferentes técnicas espectrofotométricas utilizadas para la caracterización química del nanosistema, mostró resultados de una adecuada formación del sistema AF-Fe_3O_4-IRDB, por otro lado, los experimentos de caracterización biológica fueron de igual manera adecuados.
- El sistema no mostró toxicidad importante sobre cultivos de células HeLa a concentraciones de hasta 0.5 mg mL^{-1} (con un valor de viabilidad celular mayor a 80% en todos los casos), lo cual resulta importante ya que se podría considerar el sistema multifuncional como biocompatible, aunado a esto, es importante resaltar que la concentración mayor empleada en dichos estudios resulta ser muy superior a las normalmente empleadas, para sistemas similares o diferentes, incluyendo o no fármacos modelo.

- Los estudios de captación celular mostraron una mayor captación por parte del sistema no bloqueado, esto supondría que la captación del sistema multifuncional ocurre de manera preferente mediante receptores de ácido fólico. Cabe resaltar que resulta necesario modificar los diferentes parámetros influyentes en dicho experimento (tiempo de bloqueo, concentración de solución de ácido fólico empleada para bloqueo, número de células, concentración de nanopartículas, etc.) para lograr ver una diferencia adecuada y corroborar lo obtenido o en su caso, corroborar lo contrario.
- Resulta necesario la realización de más estudios en cuánto a las características de diagnóstico que dicho sistema puede ofrecer, es decir, estudiar su comportamiento *in vitro* por técnicas de fluorescencia óptica.
- De igual manera es importante conocer las características magnéticas de dicho sistema y así poder evaluar sus potenciales usos en hipertermia.

REFERENCIAS

6. REFERENCIAS

- Adlim (2006). "Preparation and application of metal nanoparticles." Indo. J. Chem **6**(1): 1-10.
- Akbarzadeh, A., H. Mikaeili, N. Zarghami, R. Mohammad, A. Barkhordari and S. Davaran (2012). "Preparation and in vitro evaluation of doxorubicin-loaded Fe_3O_4 magnetic nanoparticles modified with biocompatible copolymers." Int J Nanomedicine **7**: 511-526.
- Anjomshoa, M., S. J. Fatemi, M. Torkzadeh-Mahani and H. Hadadzadeh (2014). "DNA- and BSA-binding studies and anticancer activity against human breast cancer cells (MCF-7) of the zinc(II) complex coordinated by 5,6-diphenyl-3-(2-pyridyl)-1,2,4-triazine." Spectrochim Acta A Mol Biomol Spectrosc **127**: 511-520.
- Banerji, B., S. K. Pramanik, S. Mandal, N. C. Maiti and K. Chaudhuri (2012). "Synthesis, characterization and cytotoxicity study of magnetic (Fe_3O_4) nanoparticles and their drug conjugate." RSC Advances **2**(6): 2493.
- Beija, M., C. A. Afonso and J. M. Martinho (2009). "Synthesis and applications of Rhodamine derivatives as fluorescent probes." Chem Soc Rev **38**(8): 2410-2433.
- Bennett, K. M., J. Jo, H. Cabral, R. Bakalova and I. Aoki (2014). "MR imaging techniques for nano-pathophysiology and theranostics." Adv Drug Deliv Rev **74**: 75-94.
- Calero, M., L. Gutierrez, G. Salas, Y. Luengo, A. Lazaro, P. Acedo, M. P. Morales, R. Miranda and A. Villanueva (2014). "Efficient and safe internalization of magnetic iron oxide nanoparticles: two fundamental requirements for biomedical applications." Nanomedicine **10**(4): 733-743.
- Calmon, M. F., A. T. de Souza, N. M. Candido, M. I. B. Raposo, S. Taboga, P. Rahal and J. G. Nery (2012). "A systematic study of transfection efficiency and cytotoxicity in HeLa cells using iron oxide nanoparticles prepared with organic and inorganic bases." Colloids and Surfaces B: Biointerfaces **100**(0): 177-184.
- Cao, H., J. He, L. Deng and X. Gao (2009). "Fabrication of cyclodextrin-functionalized superparamagnetic Fe_3O_4/amino-silane core–shell nanoparticles via layer-by-layer method." Applied Surface Science **255**(18): 7974-7980.
- Castillo, J. J., T. Rindzevicius, C. E. Rozo and A. Boisen (2015). "Adsorption and Vibrational Study of Folic Acid on Gold Nanopillar Structures Using Surface-enhanced Raman Scattering Spectroscopy." Nanomaterials and Nanotechnology: 1.
- Cutler, J. I., D. Zheng, X. Xu, D. A. Giljohann and C. A. Mirkin (2010). "Polyvalent oligonucleotide iron oxide nanoparticle "click" conjugates." Nano Lett **10**(4): 1477-1480.
- Chen, C., J. Ke, X. E. Zhou, W. Yi, J. S. Brunzelle, J. Li, E. L. Yong, H. E. Xu and K. Melcher (2013). "Structural basis for molecular recognition of folic acid by folate receptors." Nature **500**(7463): 486-489.
- Choi, K. Y., G. Liu, S. Lee and X. Chen (2012). "Theranostic nanoplatforms for simultaneous cancer imaging and therapy: current approaches and future perspectives." Nanoscale **4**(2): 330-342.
- Das, M., D. Bandyopadhyay, D. Mishra, S. Datir, P. Dhak, S. Jain, T. K. Maiti, A. Basak and P. Pramanik (2011). ""Clickable", trifunctional magnetite nanoparticles and their chemoselective biofunctionalization." Bioconjug Chem **22**(6): 1181-1193.
- Das, M., D. Mishra, T. K. Maiti, A. Basak and P. Pramanik (2008). "Bio-functionalization of magnetite nanoparticles using an aminophosphonic acid coupling agent: new, ultradispersed, iron-oxide folate nanoconjugates for cancer-specific targeting." Nanotechnology **19**(41): 415101.
- Erno Pretsch, P. B., Martin Badertscher (2009). "Structure determination of organic compounds." 444.
- Fan, Z., P. P. Fu, H. Yu and P. C. Ray (2014). "Theranostic nanomedicine for cancer detection and treatment." J Food Drug Anal **22**(1): 3-17.

- Fasting, C., C. A. Schalley, M. Weber, O. Seitz, S. Hecht, B. Koksch, J. Dernedde, C. Graf, E. W. Knapp and R. Haag (2012). "Multivalency as a chemical organization and action principle." Angew Chem Int Ed Engl **51**(42): 10472-10498.
- Gao, J. and B. Xu (2009). "Applications of nanomaterials inside cells." Nano Today **4**(1): 37-51.
- Gotić, M. and S. Musić (2007). "Mössbauer, FT-IR and FE SEM investigation of iron oxides precipitated from $FeSO_4$ solutions." Journal of Molecular Structure **834-836**: 445-453.
- Gupta, A. K. and M. Gupta (2005). "Synthesis and surface engineering of iron oxide nanoparticles for biomedical applications." Biomaterials **26**(18): 3995-4021.
- Ho, D. N., N. Kohler, A. Sigdel, R. Kalluri, J. R. Morgan, C. Xu and S. Sun (2012). "Penetration of endothelial cell coated multicellular tumor spheroids by iron oxide nanoparticles." Theranostics **2**(1): 66-75.
- Jang, B., H. Kwon, P. Katila, S. J. Lee and H. Lee (2016). "Dual delivery of biological therapeutics for multimodal and synergistic cancer therapies." Adv Drug Deliv Rev **98**: 113-133.
- Janib, S. M., A. S. Moses and J. A. MacKay (2010). "Imaging and drug delivery using theranostic nanoparticles." Adv Drug Deliv Rev **62**(11): 1052-1063.
- Kanamala, M., W. R. Wilson, M. Yang, B. D. Palmer and Z. Wu (2016). "Mechanisms and biomaterials in pH-responsive tumour targeted drug delivery: A review." Biomaterials **85**: 152-167.
- Kelemen, L. E. (2006). "The role of folate receptor alpha in cancer development, progression and treatment: cause, consequence or innocent bystander?" Int J Cancer **119**(2): 243-250.
- Kelkar, S. S. and T. M. Reineke (2011). "Theranostics: combining imaging and therapy." Bioconjug Chem **22**(10): 1879-1903.
- Kumar, C. S. and F. Mohammad (2011). "Magnetic nanomaterials for hyperthermia-based therapy and controlled drug delivery." Adv Drug Deliv Rev **63**(9): 789-808.
- Lee, H. Y., Z. Li, K. Chen, A. R. Hsu, C. Xu, J. Xie, S. Sun and X. Chen (2008). "PET/MRI dual-modality tumor imaging using arginine-glycine-aspartic (RGD)-conjugated radiolabeled iron oxide nanoparticles." J Nucl Med **49**(8): 1371-1379.
- Lu, Y. and P. S. Low (2002). "Folate-mediated delivery of macromolecular anticancer therapeutics agents." Adv Drug Deliv Rev **54**: 675-693.
- Luo, S., E. Zhang, Y. Su, T. Cheng and C. Shi (2011). "A review of NIR dyes in cancer targeting and imaging." Biomaterials **32**(29): 7127-7138.
- M., Y. K., J. Park and S. Jon (2012). "Targeting strategies for multifunctional nanoparticles in cancer imaging and therapy." Theranostics **2**(1): 3-44.
- Madru, R., P. Kjellman, F. Olsson, K. Wingardh, C. Ingvar, F. Stahlberg, J. Olsrud, J. Latt, S. Fredriksson, L. Knutsson and S. E. Strand (2012). "^{99m}Tc-labeled superparamagnetic iron oxide nanoparticles for multimodality SPECT/MRI of sentinel lymph nodes." J Nucl Med **53**(3): 459-463.
- Maggioni, D., P. Arosio, F. Orsini, A. M. Ferretti, T. Orlando, A. Manfredi, E. Ranucci, P. Ferruti, G. D'Alfonso and A. Lascialfari (2014). "Superparamagnetic iron oxide nanoparticles stabilized by a poly(amidoamine)-rhenium complex as potential theranostic probe." Dalton Trans **43**(3): 1172-1183.
- Mahmoudi, M., M. A. Sahraian, M. A. Shokrgozar and S. Laurent (2011). "Superparamagnetic iron oxide nanoparticles: promises for diagnosis and treatment of multiple sclerosis." ACS Chem Neurosci **2**(3): 118-140.
- Mahmoudi, M., S. Sant, B. Wang, S. Laurent and T. Sen (2011). "Superparamagnetic iron oxide nanoparticles (SPIONs): development, surface modification and applications in chemotherapy." Adv Drug Deliv Rev **63**(1-2): 24-46.
- Muller, C. and R. Schibli (2011). "Folic acid conjugates for nuclear imaging of folate receptor-positive cancer." J Nucl Med **52**(1): 1-4.

- Nair, B. G., T. Fukuda, T. Mizuki, T. Hanajiri and T. Maekawa (2012). "Intracellular trafficking of superparamagnetic iron oxide nanoparticles conjugated with TAT peptide: 3-dimensional electron tomography analysis." Biochem Biophys Res Commun **421**(4): 763-767.
- Palanikumar, S., L. Kannammal, B. Meenarathi and R. Anbarasan (2014). "Effect of folic acid decorated magnetic fluorescent nanoparticles on the sedimentation of starch molecules." International Nano Letters **4**(2).
- Pretsch, E., P. Bühlmann and M. Badertscher (2009). Structure determination of organic compounds: tables of spectral data. Verlag Berlin Heidelberg, Springer.
- Rahman, M. M., S. B. Khan, M. Faisal, A. M. Asiri and M. A. Tariq (2012). "Detection of aprepitant drug based on low-dimensional un-doped iron oxide nanoparticles prepared by a solution method." Electrochimica Acta **75**: 164-170.
- Reungpatthanaphong, P., S. Dechsupa, J. Meesungnoen, C. Loetchutinat and S. Mankhetkorn (2003). "Rhodamine B as a mitochondrial probe for measurement and monitoring of mitochondrial membrane potential in drug-sensitive and -resistant cells." Journal of Biochemical and Biophysical Methods **57**(1): 1-16.
- Schweiger, C., C. Pietzonka, J. Heverhagen and T. Kissel (2011). "Novel magnetic iron oxide nanoparticles coated with poly(ethylene imine)-g-poly(ethylene glycol) for potential biomedical application: synthesis, stability, cytotoxicity and MR imaging." Int J Pharm **408**(1-2): 130-137.
- Sinha, R., G. J. Kim, S. Nie and D. M. Shin (2006). "Nanotechnology in cancer therapeutics: bioconjugated nanoparticles for drug delivery." Mol Cancer Ther **5**(8): 1909-1917.
- Song, C., G. Y. Wang and D. M. Kong (2015). "A facile fluorescence method for versatile biomolecular detection based on pristine alpha-Fe_2O_3 nanoparticle-induced fluorescence quenching." Biosens Bioelectron **68**: 239-244.
- Sun, J., S. Zhou, P. Hou, Y. Yang, J. Weng, X. Li and M. Li (2007). "Synthesis and characterization of biocompatible Fe_3O_4 nanoparticles." J Biomed Mater Res A **80**(2): 333-341.
- Wen, J., S. Jiang, Z. Chen, W. Zhao, Y. Yi, R. Yang and B. Chen (2014). "Apoptosis selectively induced in BEL-7402 cells by folic acid-modified magnetic nanoparticles combined with 100 Hz magnetic field." Int J Nanomedicine **9**: 2043-2050.
- Wooley, A. M. N. a. K. L. (2011|). "The importance of chemistry in creating well-defined nanoscopic embedded therapeutics: Devices capable of the dual functions of imaging and therapy." Accounts of chemical research **44**(10): 969-978.
- Xie, C., J. Chang, X. D. Hao, J. M. Yu, H. R. Liu and X. Sun (2013). "Mitochondrial-targeted prodrug cancer therapy using a rhodamine B labeled fluorinated docetaxel." Eur J Pharm Biopharm **85**(3 Pt A): 541-549.
- Yan, C., Y. Wu, J. Feng, W. Chen, X. Liu, P. Hao, R. Yang, J. Zhang, B. Lin, Y. Xu and R. Liu (2013). "Anti-alphavbeta3 antibody guided three-step pretargeting approach using magnetoliposomes for molecular magnetic resonance imaging of breast cancer angiogenesis." Int J Nanomedicine **8**: 245-255.
- Zeinali Sehrig, F., S. Majidi, S. Asvadi, A. Hsanzadeh, S. H. Rasta, M. Emamverdy, J. Akbarzadeh, S. Jahangiri, S. Farahkhiz and A. Akbarzadeh (2015). "An update on clinical applications of magnetic nanoparticles for increasing the resolution of magnetic resonance imaging." Artif Cells Nanomed Biotechnol: 1-6.
- Zhang, C., M. Jugold, E. C. Woenne, T. Lammers, B. Morgenstern, M. M. Mueller, H. Zentgraf, M. Bock, M. Eisenhut, W. Semmler and F. Kiessling (2007). "Specific targeting of tumor angiogenesis by RGD-conjugated ultrasmall superparamagnetic iron oxide particles using a clinical 1.5-T magnetic resonance scanner." Cancer Res **67**(4): 1555-1562.